

1 **Mineral compositions of syn-collisional granitoids and their implications for**
2 **the formation of juvenile continental crust and adakitic magmatism**

3 Yuanyuan Xiao ^{1, 2*}, Shuo Chen ^{1, 2, 3}, Yaoling Niu ^{2, 4, 5}, Xiaohong Wang ^{1, 2}, Qiqi Xue ⁵,
4 Guodong Wang ⁶, Yaijie Gao ^{1, 2, 3}, Hongmei Gong ^{1, 2}, Juanjuan Kong ^{1, 2, 3}, Fengli Shao ⁷, Pu
5 Sun ^{1, 2, 3}, Meng Duan ⁵, Di Hong ^{1, 2, 3}, Dong Wang ^{1, 2, 3}

6
7 ¹ Key Laboratory of Marine Geology and Environment, Institute of Oceanology, Chinese
8 Academy of Sciences, Qingdao 266071, China; ² Laboratory for Marine Geology, Qingdao
9 National Laboratory for Marine Science and Technology, Qingdao 266061, China; ³ University
10 of Chinese Academy of Sciences, Beijing 100049, China; ⁴ Department of Earth Sciences,
11 Durham University, Durham DH1 3LE, UK; ⁵ School of Earth Science and Mineral Resources,
12 China University of Geosciences, Beijing 100083, China; ⁶ Shandong Provincial Key
13 Laboratory of Water and Soil Conservation and Environmental Protection, School of Resources
14 and Environment, Linyi University, Linyi, 276000, China; ⁷ Institute of Geology and
15 Paleontology, Linyi University, Linyi, 276000, China

16
17 Abstract (450 words), text (6452 words), 83 references, 13 figures, 13 tables and 1 figure in the
18 Supplementary information

19
20 *Corresponding author: Dr Yuanyuan XIAO. Telephone: +86-0532-82898035. Fax: +86-
21 0532-82898035. E-mail: yuanyuan.xiao@qdio.ac.cn.

22 **Abstract:**

23 Continental collision zones have been proposed as primary sites of net continental crustal
24 growth. Therefore, studies on syn-collisional granitoids with mafic magmatic enclaves (MMEs)
25 are essential for testing this hypothesis. The Baojishan (BJS) and Qumushan (QMS) syn-
26 collisional plutons in the North Qilian Orogen (NQO) on the northern margin of the Tibetan
27 Plateau have abundant MMEs in sharp contact with host granitoids, sharing similar constituent
28 minerals but with higher modal abundances of mafic minerals in MMEs. The QMS host
29 granitoids have high Sr/Y and La/Yb ratios showing adakitic compositions, different from the
30 BJS granitoids. Based on bulk-rock compositions and zircon U-Pb age dating, recent studies on
31 these two plutons proposed that MMEs represent cumulates crystallized early from the same
32 magmatic system as their host granitoids, and their parental melts are best understood as
33 andesitic magmas produced by partial melting of the underthrusting upper ocean crust upon
34 collision with some terrigenous sediments under amphibolite facies.

35 Here, we focus on trace element geochemistry of the constituent mineral phases of both
36 MMEs and their host granitoids of the QMS and BJS plutons. We show that different mineral
37 phases preferentially host different trace elements, e.g., most rare earth elements (REEs and Y)
38 reside in titanite (only found in the QMS pluton), amphibole, apatite, epidote and zircon (mostly
39 heavy-REEs), and high field strength elements (HFSEs) reside in biotite, titanite, amphibole
40 and zircon. Based on the mineral chemical data, we testify that for these two plutons, MMEs
41 are of similar cumulate origin, crystallized from primitive andesitic melts in the early stage of
42 granitoid magmatism. The primitive andesitic melts for these syn-collisional granitoids are
43 most likely produced by partial melting of the oceanic crust, supporting the hypothesis of

44 continental crustal growth considering the syn-collisional granitoids represent juvenile
45 continental crust.

46 As evidenced by distinct mineral compositions, the two plutons have different parental
47 magma compositions, e.g., higher TiO_2 content, higher Sr/Y and La/Yb ratios in the QMS
48 parental magmas, a signature best understood as being inherited from the source. The higher
49 TiO_2 content of the parental magma for the QMS pluton leads to the common presence of
50 titanite in the QMS pluton (absent in the BJS pluton), crystallization of which in turn controls
51 the trace element (REE, Y, Nb, Ta and others) systematics in the residual melts towards an
52 adakitic signature. Therefore, parental magmas with high TiO_2 content and high Sr/Y and La/Yb
53 ratios, as well as their further fractionation of titanite, are important factors in the development
54 of adakitic compositions, as represented by the QMS host granitoids. This model offers a new
55 perspective on the petrogenesis of adakitic rocks. The present study further demonstrates that
56 in general, mineral chemistry holds essential information for revealing the petrogenesis of
57 granitoid rocks.

58
59 **Keywords:** adakitic rocks; mineral chemistry; mafic magmatic enclaves; North Qilian Orogen;
60 syn-collisional granitoid petrogenesis

61 INTRODUCTION

62 The bulk continental crust is inferred to be produced by low degree partial melting of the
63 primitive mantle in Earth's early history because of the compositional complementarity
64 between incompatible element enriched continental crust and incompatible element depleted
65 oceanic crust, the depletion of which is thought to be inherited from the upper mantle, depleted
66 as the result of continental crust extraction (e.g., O'Nions *et al.*, 1979; Hofmann, 1988).
67 However, how the continental crust with andesitic composition may have derived from mantle-
68 derived basaltic magmas remains unclear. While it is widely accepted that island arcs are the
69 main building blocks responsible for the growth of the continental crust (e.g., Taylor, 1967,
70 1977), considerable amounts of the continental crustal materials have also been recognized to
71 be lost during crustal destruction by subduction removal (e.g., Stein and Scholl, 2012).
72 Meanwhile, the growth of the continental crust is episodic (e.g., Condie, 1998). Hence, the
73 "Island-arc" model (Taylor, 1967, 1977) may not be responsible for continental crustal growth.
74 On the basis of studies of the syn-collisional andesites and granitoids from southern Tibet (Niu
75 *et al.*, 2007; Mo *et al.*, 2008), Niu *et al.* (2013) proposed that continental collision zones are
76 primary sites for net continental crust growth. Importantly, Niu *et al.* (2013) demonstrates that
77 syn-collisional andesites and granitoids show remarkable similarity to bulk continental crustal
78 compositions in all the major and trace element abundances and ratios, suggesting that syn-
79 collisional granitoids represent juvenile continental crust resulting from partial melting of the
80 subducting/subducted upper oceanic crust with minor terrigenous sediments under amphibolite
81 facies (Mo *et al.*, 2008; Niu & O'Hara, 2009; Niu *et al.*, 2013). Studies on the petrogenesis of
82 syn-collisional granitoids are important for testing this hypothesis. Our studies on syn-

83 collisional granitoids with mafic magmatic enclaves (MMEs) from orogens on the Tibetan
84 Plateau and adjacent regions (e.g., Qinling, Kunlun and Qilian orogens) support this hypothesis
85 in many aspects, including significant mantle Nd-Hf isotopic contributions to the granitoids
86 (Huang *et al.*, 2014, 2015, 2016, 2017; Chen *et al.*, 2015, 2016, 2018; Li *et al.*, 2016, 2017;
87 Duan *et al.*, 2016; Zhang *et al.*, 2016; Kong *et al.*, 2017). Nevertheless, quantification is
88 necessary in order to develop this testable hypothesis into a comprehensive theory. This requires
89 refined experimental petrology on oceanic crust melting in the context of continental collision
90 and detailed major and trace element systematics in the constituent minerals of syn-collisional
91 granitoids and the hosted MMEs.

92 As magmatic products, the mineralogy and mineral compositions hold the key to magmatic
93 conditions and processes (e.g., Sha & Chappell, 1999; Belousova *et al.*, 2002a; Hoskin &
94 Schaltegger, 2003; Piccoli *et al.*, 2011; Bruand *et al.*, 2019), such as oxygen fugacity (e.g.,
95 Belousova *et al.*, 2002b), magma mixing (McLeod *et al.*, 2011; Bruand *et al.*, 2014; Laurent *et*
96 *al.*, 2017; Hu *et al.*, 2017), fractional crystallization (Marks *et al.*, 2008) and subsequent
97 metasomatism (e.g., Smith *et al.*, 2009). Comprehensive geochemical studies on both major
98 and accessory minerals are thus necessary to genuinely understand the petrogenesis of igneous
99 rocks (e.g., Bachmann *et al.*, 2005; Gao *et al.*, 2009). In this paper, we present mineral *in situ*
100 trace element data on two well-characterized syn-collisional granitoid plutons, i.e., the
101 Baojishan (BJS) and Qumushan (QMS) plutons in the North Qilian Orogen (NQO) on the
102 northern margin of the Tibetan Plateau (Chen *et al.*, 2015, 2016, 2018). Both QMS and BJS
103 plutons have similarly abundant MMEs in sharp contact with host granitoids, while the QMS
104 host granitoids show adakitic characteristics, which is different from the QMS MMEs or the

105 BJS granitoids (Chen *et al.*, 2015, 2016). Although the adakitic QMS host granitoids have been
106 interpreted as resulting from fractional crystallization of primitive andesitic magmas (Chen *et*
107 *al.*, 2016), it needs quantifying by considering detailed and specific controls of different
108 crystallized minerals in the granitoid systems. Our data provide further constraints on the
109 petrogenesis of MMEs in the context of syn-collisional granitoid magmatism, and also help
110 explain why the QMS host granitoids have adakitic compositions, whereas the BJS granitoids
111 do not, offering new insights into the widely discussed and debated origin of adakite and
112 adakitic rocks.

113 **GEOLOGICAL BACKGROUND AND PETROLOGY**

114 The NQO at the northern margin of the Tibetan Plateau is an early Paleozoic suture zone
115 formed through the subduction of the Qilian seafloor and subsequent collision between the
116 Alashan Block and the Qilian-Qaidam Block (Fig. 1a,b; Song *et al.*, 2006, 2013, 2014a,b). It
117 comprises the southern and northern ophiolite belts, separated by an island-arc igneous complex.
118 The ophiolite in the southern belt is thought to represent the ocean crust formed at the ocean
119 ridge, while the ophiolite in the northern belt is of a back-arc basin origin (Fig. 1a,b; Xia *et al.*,
120 2003, 2012; Xia & Song, 2010; Song *et al.*, 2013; Xiao *et al.*, 2013). The Qilian ocean basin is
121 thought to be formed since *c.* 710 Ma with a recorded seafloor subduction history between *c.*
122 520 and *c.* 440 Ma, just prior to continental collision (Song *et al.*, 2013). The BJS and QMS
123 granitoid plutons are located in the northern ophiolite belt of the eastern NQO. Both BJS and
124 QMS plutons show a zircon U-Pb crystallization age of *c.* 430 Ma (Chen *et al.*, 2015, 2016),
125 which is consistent with the timing of continental collision (i.e., *c.* 440 – 420 Ma; Song *et al.*,
126 2009, 2013).

127 The BJS and QMS plutons contain abundant MMEs of varying shape and size (a few to
128 tens of centimeters in diameter) in sharp contact with their host granitoids (Fig. 1c,d). The hosts
129 of both plutons are granodioritic, mainly composed of plagioclase (*c.* 40 – 50 %) + quartz (*c.*
130 20 – 30 %) + biotite (*c.* 10 – 20 %) + amphibole (*c.* 5 – 10 %; Fig. 2). The MMEs are dioritic
131 with the same mineralogy as their host, but have finer grain size and greater modal amphibole,
132 less modal plagioclase and quartz, i.e., amphibole (*c.* 25 – 45 %) + biotite (*c.* 15 – 20 %) +
133 plagioclase (*c.* 20 – 40 %) + quartz (*c.* 5 – 10 %; Fig. 2). Pyroxene is not found in the MMEs
134 and their host granitoids in either pluton. Accessory minerals are mainly apatite, epidote, titanite,
135 zircon, muscovite and K-feldspar with varying modal abundances in both MMEs and their host
136 plutons (Fig. 2). Among others, epidote is more common in the BJS pluton (especially in host
137 granodiorites; e.g., Fig. 2a-c), while apatite is more common in the QMS pluton. Titanite (up to
138 *c.* 500 μm in length) is only found in the QMS pluton (e.g., Fig. 2e-h). Apatite crystals are
139 always euhedral. Epidote crystals are anhedral, and some of them occur as inclusions in
140 amphibole. Titanite is anhedral and shows varying colored patches.

141 ANALYTICAL METHODS

142 MMEs and their host granitoids of the QMS and BJS plutons were prepared as 60 μm
143 thick sections, and major and accessory minerals were analyzed using LA-ICP-MS in the
144 Laboratory of Ocean Lithosphere and Mantle Dynamics (LOLMD) at the Institute of
145 Oceanology, Chinese Academy of Sciences. We used a 193 nm ultra-short pulse excimer laser
146 ablation system (Analyte Excite produced by Photon-machines Company) coupled with an
147 Agilent 7900 ICP-MS instrument. Operation conditions of LA-ICP-MS analysis are
148 summarized in Table DR2 (see details in caption of Fig. DR1). Considering the relatively

149 homogeneous compositions of igneous minerals, a large spot size of 40 μm was used with a
150 low energy density (4.72 J/cm²) to ensure fractionation with increasing ablation depths was
151 minimized. During each run, fifty-three elements, including both major and trace elements,
152 were analyzed. Acquisition times for background (gas blank) and subsequent sampling were 25
153 s and 50 s, respectively. The Agilent Chemstation was utilized for the acquisition of each
154 individual analysis.

155 Off-line data reduction, including signal selection, drift correction and quantitative
156 calibration was done using ICPMSDataCal (Liu *et al.*, 2008; Lin *et al.*, 2016). For anhydrous
157 minerals (feldspar, titanite and zircon), all the analyzed elements in each run were normalized
158 to 100 % and calibrated using an ablation yield correction factor (AYCF; Liu *et al.*, 2008) based
159 on analysis of multiple reference materials, i.e., NIST SRM 610, USGS BCR-2G, BIR-1G,
160 BHVO-2G and a synthesized glass GSE-1G (Jochum *et al.*, 2005). For hydrous minerals
161 (amphibole, biotite, epidote, apatite, muscovite and carbonate), we chose ⁴²Ca (for apatite and
162 carbonate) and ²⁸Si (for silicate minerals) as the internal standards for data calibration, which
163 were previously analyzed using an electron probe micro-analyzer (EPMA; Chen *et al.*, 2015,
164 2016). In some cases, we instead used mineral compositional data from the rocks with similar
165 composition and mineralogy to our rocks from the literature (Dahlquist, 2002; Tables
166 DR3,4,6,7,9). Each batch of sample analysis started and ended with the analysis of the multiple
167 reference materials (i.e., NIST SRM 610, USGS BCR-2G, BIR-1G, BHVO-2G and GSE-1G).
168 Analysis of every five samples was bracketed with analysis of GSE-1G twice, one of which
169 was used for monitoring drift and applying drift correction (if any), the other indicating the
170 analytical precision and accuracy, i.e., within 5 % and below 10 % respectively for most

171 analyzed elements (Fig. DR1; recommended values are referred to GeoReM). During the
172 analysis, we purposely chose spots of fresh areas and avoided other mineral inclusions to ensure
173 representativeness of the analyzed mineral compositions.

174 **RESULTS**

175 Mineral chemical data for both MMEs and their host granodiorites from both plutons are
176 summarized in Tables DR3-9, and primitive mantle normalized trace element data for these
177 minerals are presented in Fig. 3b-h, with the primitive mantle normalized trace element diagram
178 for the average bulk rock compositions for comparison (Fig. 3a).

179 **Amphibole**

180 Amphibole from the QMS pluton has higher Mg# (63.2 to 70.4 vs. 53.8 to 62.5) and lower
181 Al₂O₃ (4.63 – 8.49 wt.% vs. 7.33 – 10.56 wt.%) than that from the BJS pluton (Fig. 4; Table
182 DR3). The QMS amphibole contains higher light rare earth elements (LREEs) and lower heavy
183 rare earth elements (HREEs)-Y than the BJS amphibole (e.g., [La/Yb]_N = 2.03 – 7.08 vs. 0.19
184 – 1.81; Fig. 3b), consistent with greater LREE/HREE fractionation in the QMS bulk rocks (Fig.
185 3a and Table DR1). The QMS amphibole has higher Nb/Ta than the BJS amphibole (Figs.
186 3b&4g and Table DR3). The QMS amphibole also has higher Ni and lower Sc contents than
187 the BJS amphibole (Fig. 4h). Amphiboles in MMEs contain consistently higher Ni-Cr and lower
188 Sc than those of their host granitoids in both plutons (e.g., Fig. 4h) but share similar contents
189 for most other analyzed trace elements (Table DR3).

190 **Biotite**

191 Biotite from the QMS pluton shows higher Mg# (59.3 to 64.2 vs. 52.6 to 58.6) and lower

192 Al₂O₃ (13.45 to 15.22% vs. 14.82 to 16.71%) than that of the BJS pluton (Fig. 5; Table DR4).
193 Both QMS and BJS biotite contains high Ba-Rb-Cs-K, *c.* 1000 times the primitive mantle
194 values (Fig. 3c). The QMS biotite has somewhat higher LREEs-Sr contents and much lower Ta
195 (Fig. 3c) with higher Nb/Ta ratios (Fig. 5a-b,d) than the BJS biotite (Table DR4). Furthermore,
196 Nb/Ta ratios of biotite slightly decrease rimwards (Fig. 5a,b). Some small muscovite crystals
197 (Fig. 2a) were also analyzed, containing the highest Rb contents of all analyzed minerals, up to
198 731 ppm (Table DR4). For both plutons, biotites from MMEs show a similar composition to
199 those of their host granitoids (Table DR4).

200 **Feldspar**

201 Plagioclase An% (Ca/[Ca+Na+K]) values gently decrease toward crystal rims (Fig. 6a-d),
202 and the QMS plagioclase has lower An values than that in the BJS pluton (Fig. 6e-h), 22% vs.
203 39% on average (Table DR5). Plagioclase has high Pb, Sr, Ba, Cs and LREEs contents (Fig.
204 3c), which generally decrease with decreasing An (Fig. 6e-h), except gentle increase of Ba for
205 the BJS plagioclase (Fig. 6f). Plagioclase in the QMS pluton shows obviously higher Ba-Cs-Sr
206 and lower Y than that in the BJS pluton (e.g., Figs. 3d&6e-h), consistent with such differences
207 in bulk rocks between the two plutons (Fig. 3a; Table DR1). For both plutons, plagioclase from
208 MMEs show similar compositions to those of their host granitoids (Fig. 3d; Table DR5).

209 **Apatite**

210 Apatite contains consistently high Th, U and REEs contents, *c.* 1000 times the primitive
211 mantle values (Fig. 3e). Apatite from the QMS pluton shows higher LREEs, lower HREEs and
212 thus higher [La/Yb]_N than that in the BJS pluton (Fig. 3e and Table DR6), which is consistent
213 with what is observed in the bulk rocks (Fig. 3a; Table DR1).

214 **Epidote**

215 Epidote contains the highest Sr and Pb contents of all analyzed minerals (*c.* 100 and *c.*
216 1000 times primitive mantle values, respectively; Fig. 3f). Because of small grain sizes, epidote
217 in MMEs of the QMS pluton was not analyzed. Epidote from the QMS host granitoids has
218 higher Sr and LREEs and lower HREEs than that from the BJS pluton (Fig. 3f), consistent with
219 the bulk-rock compositions (Fig. 3a).

220 **Titanite**

221 Titanite is only found in host and MMEs of the QMS pluton and has the highest Nb-Ta-
222 Ti-Th-U-LREEs contents of all minerals analyzed, up to *c.* 10⁴ times the primitive mantle values
223 (Fig. 3g). Some titanite crystals show great variations in color and composition, with firtree-
224 like zoning or patches and can be divided into two parts, i.e., more reddish parts and less reddish
225 parts (Fig. 7). The more reddish parts show higher Nb-Ta-Zr-Hf-Th-U-Pb-REE-Y contents to
226 variable extents (e.g., Figs. 7&8; Table DR8), but their LREE/HREE (e.g., La/Yb) and Th/U
227 ratios generally overlap with those of the less reddish parts (Fig. 8d). No obvious titanite
228 compositional differences exists between MMEs and their host rocks (Figs. 3g&8).

229 **Others (zircon and carbonate)**

230 Our *in situ* mineral analysis in thin sections (Table DR9) and previous analysis on zircon
231 separates (Chen *et al.*, 2015, 2016; Table DR10) show that zircon has the highest Zr-Hf-HREE
232 contents and the lowest [LREE/HREE]_N among all the minerals analyzed (Fig. 3h; Tables
233 DR9&10), e.g., *c.* 10³ times the primitive mantle values for HREEs. Relative to the BJS zircon,
234 the QMS zircon has generally higher Th-U-LREE contents with relatively higher
235 [LREE/HREE]_N and Th/U ratios (0.7 vs. 0.4 on average), and lower Eu/Eu* (=

236 $\text{Eu}_N/[\text{Sm}_N \times \text{Gd}_N]^{1/2}$, 0.55 vs. 0.61 on average) and Ce/Ce^* values ($= \text{Ce}_N/[\text{La}_N \times \text{Pr}_N]^{1/2}$, 71 vs.
237 125 on average; Fig. 3h; Tables DR9&10). Some small carbonate crystals are analyzed to show
238 high Sr (up to c. 400 ppm) and variably high LREEs and U (Table DR9).

239 **DISCUSSION**

240 **Identifying trace element budgets**

241 Previous studies have reported that accessory minerals (mainly focused on titanite, apatite
242 and zircon) can be significant trace element hosts (especially for REEs and high field strength
243 elements [HFSEs]; e.g., Sha & Chappell, 1999; Tiepolo *et al.*, 2002; Belousova *et al.*, 2002a,b;
244 Hoskin and Schaltegger, 2003; Marks *et al.*, 2008; McLeod *et al.*, 2011; Piccoli *et al.*, 2011;
245 Bruand *et al.*, 2014). To better understand how elements are controlled by different minerals,
246 we reconstructed element budgets for average bulk-rock compositions of the MMEs and their
247 host granitoids from the BJS and QMS plutons using average mineral compositions and modal
248 mineralogy (Table DR11) normalized to averaged values of analyzed element contents in bulk
249 rocks (Fig. 9). Modal proportions for amphibole-plagioclase-biotite-epidote-apatite-titanite-
250 carbonate-zircon are estimated using average bulk-rock major element contents through
251 Cramer's rule (see details in Table DR11). Considering that Si is the only major component for
252 quartz, the proportion of quartz is simply calculated by using 1 minus the sum of other mineral
253 proportions. The estimated mineral proportions are consistent with our petrologic observations,
254 suggesting both are reliable. Some large uncertainties for trace element budgets are caused by
255 uncertainties associated with modal estimation and mineral compositional variations at both
256 crystal and bulk-rock scales. The compositional reconstruction in Fig. 9 is useful for
257 understanding trace element distribution between phases (Table DR12) in the bulk-rock make-

258 up, which is essential in correctly interpreting the petrogenesis.

259 Different trace elements have their phase preference. For example, elements K-Rb-Cs-Ba
260 are dominantly hosted in biotite; Pb-Sr in feldspar and epidote; Th-U-REEs-Y mainly in
261 amphibole, titanite (only found in the QMS pluton), apatite and epidote; Nb-Ta-Zr-Hf in titanite,
262 zircon (also for some HREEs) and amphibole; transition metals (e.g., Sc-V-Cr-Ni) mainly in
263 amphibole and biotite. Biotite is also an important host for Ti-Nb-Ta. All these indicate that
264 accessory minerals, such as titanite, apatite, zircon and epidote, are as important as major
265 minerals in hosting their preferred trace elements in bulk rocks. The understanding on trace
266 element budgets forms the basis for understanding which mineral fractionation can control what
267 geochemical variations during magma evolution. In the following, we use this knowledge to
268 discuss the petrogenesis of MMEs and their host granitoids for the QMS and BJS plutons.

269 **Genetic link between the QMS and BJS plutons and the formation of MMEs**

270 *Petrogenesis of MMEs and syn-collisional granitoids*

271 Strictly speaking, granitoids like other intrusive rocks do not represent melts, but
272 “mechanical” mixtures of solidified “interstitial” melts and crystalline phases (Niu, 2005).
273 Hence, the bulk-rock composition of granitoids is largely determined by the type and mode of
274 minerals present. It follows that mineral-mode controlled bulk-rock composition alone may not
275 provide unique information on the parental magmas. Because minerals must be in equilibrium
276 with the melt from which they crystallize, mineral compositions thus directly record the melt
277 compositions. Therefore, both mineral chemistry and bulk-rock composition are required to
278 constrain the petrogenesis of these granitoids and their MMEs, including the compositions of
279 their parental magmas, magma sources, as well as the petrogenetic processes operating.

280 Both BJS and QMS syn-collisional granitoid plutons are situated in the eastern NQO (Fig.
281 1b). They were produced in the same tectonic setting through the same process and at the same
282 time (the same zircon crystallization age of *c.* 430 Ma; Chen *et al.*, 2015, 2016). Specifically,
283 the MMEs and host granitoids of both plutons have similar mineral assemblages with more
284 abundant mafic phases in MMEs than their host, and share similarly high large ion lithophile
285 elements (LILEs) and low HFSEs with relatively flat HREE patterns (Fig. 3a) and positive ϵ_{HF}
286 (t) values (Chen *et al.*, 2015, 2016). Based on these geochemical features, Chen *et al.* (2015,
287 2016) concluded that primitive magmas parental to both plutons resulted from partial melting
288 of the underthrusting upper oceanic crust upon collision, with minor terrigenous sediment
289 contributions under amphibolite facies (Niu *et al.*, 2013; Fig. 10).

290 For the formation of MMEs, different models have been proposed in the literature. The
291 MMEs are thought to represent mantle-derived basaltic magmas mixing with granitic magmas
292 (e.g., Vernon, 1984; Chen *et al.*, 2009; McLeod *et al.*, 2011; Bruand *et al.*, 2014), refractory
293 restite after granitic magma extraction (e.g., Chappell and White, 1991), or early crystallized
294 mafic cumulate fragments dispersed in the co-genetic granitic magmas (e.g., Dahlquist, 2002;
295 Niu *et al.*, 2013). Specifically, for the BJS and QMS plutons, the compositional similarity of
296 minerals from MMEs and their host granitoids shown in this study (Figs. 3-8) indicates that
297 both the MMEs and their host granitoids share common parental magmas, with their mineral
298 compositions strongly dependent on parental magma compositions. The generally overlapping
299 mineral compositions are inconsistent with MMEs being of restite origin or external origin (e.g.,
300 Hu *et al.*, 2017). Furthermore, the relatively uniform compositions for all the analyzed
301 individual mineral crystals (i.e., rather weak core-to-rim variations without complex zoning;

302 Figs. 4-7) indicate the absence of disequilibrium, arguing against a magma-mixing origin of the
303 MMEs (Browne *et al.*, 2006; Chen *et al.*, 2009; Bruand *et al.*, 2014; McLeod *et al.*, 2011;
304 Laurent *et al.*, 2017). Hence, our new mineral data support that MMEs and respective host
305 granitoids share the same parental magmas. This is consistent with the results of previous
306 studies (Chen *et al.*, 2015, 2016) on bulk-rock geochemistry (e.g., uniform Sr-Nd-Hf isotopic
307 composition) and the same zircon U-Pb age of MMEs and host granitoids for these two plutons.

308 Our studied MMEs show a finer grain size than their host granitoids, which is in fact
309 consistent with an earlier cumulate origin of the same magmatic systems if we consider the
310 process of magma emplacement, “magma chamber” development and evolution (Fig. 10).
311 When the primitive magmas intrude into the “cold” crust to develop a magma chamber, rapid
312 cooling can significantly enhance crystal nucleation and result in the crystallization of fine-
313 grained cumulates dominated by mafic minerals near the walls and base of the magma chamber.
314 These fine-grained cumulates are later dispersed as MMEs in the slowly cooling magma bodies
315 that solidified as the coarse-grained granitoid host. Hence, fine-grained MMEs of cumulate
316 origin can be present in the host granitoid through this process.

317 Despite the similarities in bulk-rock incompatible element patterns (Fig. 3a) and mineral
318 compositions (Figs. 3-8) between MMEs and host granitoids as a result of their same parental
319 magma, MMEs also show some compositional differences from their host granitoids in the BJS
320 and QMS plutons, e.g., significantly higher middle (M)-HREE contents (Fig. 3a) and Sc-V-Cr-
321 Ni (Table DR1). These differences are in fact controlled by their high modal amphibole content,
322 as these elements are less incompatible in amphibole (e.g., Bottazzi *et al.*, 1999; Tang *et al.*,
323 2017; Zhang *et al.*, 2019), which is consistent with amphibole to be the primary host mineral

324 for M-HREEs in our modelling results (Table DR11 and Fig. 9), and our petrologic observations
325 (Fig. 2). The slight differences of LREEs between MMEs and host granitoids from the QMS
326 (Fig. 3a) are caused by titanite, which is only present in the QMS. Hence, bulk-rock REE
327 variations between MMEs and their host granitoids for both the QMS and BJS plutons are
328 controlled by different modal abundances of amphibole (and titanite also for the QMS pluton),
329 i.e., more amphibole and titanite for higher REEs in the MMEs. Similarly, the bulk-rock
330 variations of Sc-V-Cr-Ni between MMEs and their host granitoids for the two plutons (Table
331 DR1) result from the varying modal abundances of amphibole and biotite, which are the most
332 important minerals for hosting these elements (Fig. 9). All of these chemical characteristics are
333 consistent with the much stronger fractionation of these minerals (e.g., amphibole, biotite) at
334 earlier stages of magma evolution, in support of MMEs representing the early cumulate formed
335 from the same magmatic system, followed by the formation of their host granitoids.

336 *Implications on continental crustal growth*

337 Experimental studies have shown that Fe/Mg ratios of amphibole positively correlate with
338 that of their equilibrium andesitic melt and that the amphibole Mg# systematically decreases
339 with decreasing temperature during magma fractionation at both low- and high-pressure
340 conditions (Alonso-Perez *et al.*, 2009). Thus, the amphibole Mg# can be used to evaluate the
341 Mg# and degree of fractionation of the equilibrium melt, which reflects whether amphibole
342 formed from primary basaltic melts or andesitic melts (Carmichael, 2002; Hidalgo & Rooney,
343 2010; Rooney *et al.*, 2011; Tiepolo *et al.*, 2012; Ribeiro *et al.*, 2016).

344 The overlapping Mg# values of our analyzed amphibole from MMEs and host granitoids
345 also indicate the same parental magma for MMEs and host granitoids in each pluton (Fig. 4).

346 These analyzed Mg# values (i.e., 63 – 70 for the QMS amphibole and 54 - 63 for the BJS
347 amphibole) overlap with those of the liquidus amphiboles in experiments on andesitic melts (<
348 65; Alonso-Perez *et al.*, 2009; Prouteau and Scaillet, 2013), indicating that MMEs and host
349 granitoids of the two plutons are derived from andesitic melts. Although andesitic melts can
350 also result from the evolution of basaltic melts, the observed mineral assemblage of amphibole
351 and feldspar without pyroxene, together with the positive $\epsilon_{\text{HF}}(t)$ values (mantle signature) of
352 these rocks (Chen *et al.*, 2015, 2016) and recent modelling for the fractionation effects of NQO
353 syn-collisional granitoids (Chen *et al.*, 2018) suggest that parental magmas for syn-collisional
354 granitoids from these two plutons are most likely primitive andesitic melts. Importantly, the
355 volume of andesitic melts as the result of basaltic magma evolution is minor and the
356 fractionation of basaltic magmas cannot produce volumetrically rather significant (on the order
357 of *c.* $10^5 - 10^6 \text{ km}^3$) syn-collisional granitoids along each and every orogenic belt we studied
358 and globally (Niu, 2005; Niu *et al.*, 2013). Hence, our new data on mineral compositions further
359 support that these syn-collisional granitoids result from primitive andesitic magmas produced
360 by partial melting of the underthrusting oceanic crust in response to continental collision (Fig.
361 10), which can contribute to the net continental crust growth if these syn-collisional granitoids
362 are preserved in continental collision zones (Mo *et al.*, 2008; Niu & O'Hara, 2009; Niu *et al.*,
363 2013; Chen *et al.*, 2015, 2016, 2018).

364 **Geochemical differences between the QMS and BJS plutons and the adakitic**
365 **characteristics of the QMS host granitoids**

366 *Compositionally distinct parental magmas for the two plutons*

367 Although the QMS and BJS plutons share a common tectonic setting in space and time

368 as discussed above, bulk-rock compositions of the QMS granitoids and MMEs are clearly
369 different from those of the respective BJS granitoids and MMEs, e.g., the QMS granitoids and
370 MMEs have higher Mg#, TiO₂, REEs and HFSEs with higher LREE/HREE ratios and lower
371 CaO (Fig. 3a and Table DR1; Chen *et al.*, 2015, 2016). The same mineral phases in the two
372 plutons also show systematic differences accordingly (Figs 4-6, 11). Amphibole and biotite in
373 the QMS pluton have higher Mg# (Figs. 4-5), while feldspar exhibits lower An % (Fig. 6). The
374 REE-hosting minerals (i.e., amphibole, apatite, epidote and zircon) in the QMS pluton show
375 generally higher LREE/HREE ratios than those in the BJS pluton (Figs. 3&11). Biotite and
376 amphibole, which are important hosts for Nb and Ta, in the QMS plutons have similar Nb
377 contents but variably lower Ta contents than those in the BJS pluton (Tables DR3 and DR4),
378 resulting in characteristically higher Nb/Ta ratios of these two minerals from the QMS pluton
379 (Figs. 3b,c&4g&5d). Hence, the bulk-rock chemical differences between MMEs and host
380 granitoids are controlled by varied modal mineralogy as a consequence of magma evolution
381 (e.g., more amphibole crystallized in MMEs responsible for higher REE contents of MMEs),
382 while it is the mineral compositional differences between QMS and BJS plutons that determine
383 the bulk-rock compositional differences between the two plutons. Because mineral
384 compositions record the compositions of melts in equilibrium with the minerals, these
385 systematic mineral compositional differences (e.g., Figs. 3-8) indicate that the two plutons
386 evolved from compositionally different parental magmas.

387 Because amphibole as the liquidus phase has “similar” chemistry to andesitic magmas, it
388 can be used to constrain the parental melt compositions (Hidalgo *et al.*, 2007; Tiepolo *et al.*,
389 2012; Chambefort *et al.*, 2013; Ribeiro *et al.*, 2016; Tang *et al.*, 2017). Considering the effect

390 of melt compositions, we used partition coefficients between amphibole and basaltic-andesitic
391 melts (data source from <https://earthref.org/GERM/> and Hidalgo *et al.*, 2007; Table DR13) to
392 calculate trace element compositions of the melt in equilibrium with the amphibole. The
393 calculated compositions of melt in equilibrium with the QMS amphibole show greater REE
394 fractionation (e.g., give the range of $[La/Yb]_N > 7.58 - 26.4$ vs. $0.72 - 6.75$ for the BJS
395 equilibrium melt) and higher Sr/Y ratios than those for the BJS pluton (Figs. 12&13). Therefore,
396 this further demonstrates that the andesitic magmas parental to the two plutons are distinctly
397 different, reflecting compositional differences of their magma source.

398 *The adakitic characteristics of the QMS host granitoid*

399 “Adakite” is defined by its distinctive geochemical signatures, i.e., high SiO₂ (≥ 56 wt.%),
400 Al₂O₃ (≥ 15 wt.%), Sr (> 400 ppm), Sr/Y (> 40) and La/Yb ratios (> 20), low Y (< 18 ppm)
401 and HREEs (Yb < 1.9 ppm), and is originally thought to be produced by melting of young (no
402 older than 25 Ma) and warm subducting oceanic crust under eclogite or garnet amphibolite
403 facies conditions (Defant & Drummond, 1990). However, recent studies have found that
404 adakitic rocks can be produced in different tectonic settings through different geological
405 processes, e.g., mixing of basaltic and felsic magmas (Chen *et al.*, 2013; Streck *et al.*, 2007),
406 melting of mafic lower crust (Gao *et al.*, 2004; Chung *et al.*, 2003), and fractional crystallization
407 of parental basaltic magmas (e.g., Castillo *et al.*, 1999, 2012; Wang *et al.*, 2005, 2007;
408 Macpherson *et al.*, 2006; Rodríguez *et al.*, 2007; Ribeiro *et al.*, 2016).

409 The QMS host granitoids show adakitic characteristics, i.e., high Sr/Y and La/Yb ratios (89
410 and 33 on average, respectively; Fig. 13 and Table DR1), which is different from the QMS
411 MMEs or the BJS granitoids. In this study, we discuss detailed and specific controls of all the

412 crystallized minerals such as amphibole, plagioclase, biotite, apatite, zircon, titanite, epidote in
413 the granitoid systems as illustrated in Fig. 13. The bulk-rock MMEs and host granitoids of the
414 QMS pluton consistently show higher Sr/Y and La/Yb ratios than those of the BJS pluton (Fig.
415 13; Chen *et al.*, 2015, 2016), which is also true for their constituent minerals (e.g., amphibole,
416 biotite, plagioclase and apatite; Fig. 11&13d, Tables DR3-9). In Fig. 13, the high Sr/Y and
417 La/Yb ratios of the calculated melts in equilibrium with the MME amphiboles for the QMS
418 pluton resemble adakitic compositions, while those for the BJS pluton do not, reflecting that
419 the parental magma of the QMS pluton had high Sr/Y and La/Yb ratios. Thus, the systematic
420 differences of Sr/Y and La/Yb ratios in both bulk-rock and mineral compositions between the
421 two plutons (Figs. 11-13) must have been inherited from their different parental magmas. All
422 these observations demonstrate explicitly that compositions of parental magmas exert a primary
423 control on whether they have the potential to evolve to adakitic compositions.

424 Despite the relatively higher Sr/Y and La/Yb ratios of the parental magma for the QMS
425 pluton, it is the host granitoid, not the MMEs, of the QMS pluton that clearly shows adakitic
426 characteristics (Fig. 13a,b; Table DR1). The Sr/Y and La/Yb ratios of MMEs are lower than
427 their parental magmas (Fig. 13a,b). This is consistent with the understanding that the MMEs do
428 not represent melt compositions but are of cumulate origin. This, in turn, indicates that primitive
429 andesitic melts parental to the QMS granitoid with high La/Yb and Sr/Y can further evolve into
430 adakitic melts through fractional crystallization of the MME mineral assemblage. This MME
431 fractionation that leads to adakitic melts is modelled in Fig. 13. For this, we (1) assume the
432 parental andesitic melts are in equilibrium with the MME amphibole of the QMS pluton, (2)
433 apply Rayleigh fractional crystallization, and (3) use the modelled mineral modal abundances

434 in the QMS MMEs (Table DR11) to approximate the co-precipitating phase assemblage of 25%
435 amphibole + 45% plagioclase + 20% biotite + 1.7% apatite + 0.5% titanite + 2.4% epidote +
436 0.03% zircon, which is generally consistent with the petrographic observation (Fig. 2). Note
437 that the bulk-rock compositions of the MMEs and samples of their host granitoid plot in
438 complement with respect to the model parental melt, which is best illustrated in Fig. 13a.

439 Modelling shows that about 20% fractionation of the melts can produce the high Sr/Y and
440 La/Yb ratios observed in the QMS host rocks (Fig. 13). Considering the mineral fractionation
441 model in Fig. 13a, 0.1 – 0.2 % titanite fractionation is enough to increase Sr/Y ratios in the
442 melts to be as high as in the QMS host rocks, which is consistent with the very low Sr/Y ratios
443 of titanite (*c.* 0.02; Fig. 13d and Table DR8) and its relatively common presence in the QMS
444 pluton (Fig. 2e-h). Amphibole (< 40%) and zircon (< 1%) fractionation can also lead to the
445 increase of Sr/Y ratios in the melts as high as the values of the QMS host rocks (Fig. 13a). The
446 effect of apatite fractionation is insignificant, i.e., *c.* 5 – 7% apatite is required to increase Sr/Y
447 ratios in the melts to be similar to the values of the QMS host rocks (Fig. 13a), which is not
448 supported by apatite modal abundances (no more than 2% based on the analyzed P₂O₅ contents
449 of bulk rocks, Table DR11). In addition, considering zircon (with [La/Yb]_N << 1.0) and titanite
450 have the highest Yb contents (up to hundreds of ppm) among all the minerals analyzed (Fig. 3
451 and Tables DR8,9), 0.2% titanite or zircon can lead to the increase of La/Yb ratios to be as high
452 as in the QMS host rocks (Fig. 13b). No more than 40% amphibole fractionation will result in
453 the observed increase of La/Yb ratios in the melts. All of these are consistent with our modelled
454 mineral modal abundances of the QMS MMEs (Table DR11) and much lower Sr/Y and La/Yb
455 ratios of these minerals than in primitive melts parental to the QMS pluton (Figs. 8e,f, 11, 13d).

456 Furthermore, Eu/Eu^* values of the melts can also increase correspondingly with the
457 fractionation of titanite (0.2 %), according to the Eu/Eu^* difference we observed between
458 MMEs and their host granitoids of the QMS pluton (Fig. 13c).

459 Considering the distinction of mineral assemblages between the two plutons, i.e., the
460 common presence of titanite in the QMS pluton and the absence of titanite in the BJS pluton
461 (Table DR11), our data indicate that the fractionation of titanite is the most important mineral
462 to effectively increase both Sr/Y and La/Yb ratios in the residual melts and is most likely
463 required for the formation of the adakitic characteristics of the QMS host rocks (Figs. 10&13).
464 Although amphibole fractionation can also result in the increase of Sr/Y and La/Yb ratios in the
465 residual melts, the higher degree of amphibole fractionation in the BJS pluton than in the QMS
466 pluton (e.g., 44% vs. 25% in MMEs in the modelling, Table DR11) is expected to result in even
467 greater increases of Sr/Y and La/Yb ratios, which are inconsistent with the observed lower Sr/Y
468 and La/Yb ratios in the BJS host granitoids (Fig. 13a,b). Thus, the effect of the amphibole
469 fractionation to cause the adakitic signatures is not as important as that of the titanite
470 fractionation. Although plagioclase crystallization will tend to decrease La/Yb and especially
471 Sr/Y ratios in the residual melts, its effect on these ratios may have been suppressed by the
472 fractionation of other minerals such as titanite and amphibole (Fig. 13).

473 Titanite crystallization may be controlled by magmatic conditions. However, because both
474 BJS and QMS granitoids are produced by partial melting of the underthrusting oceanic crust in
475 response to continental collision under the amphibolite facies at the same time, it is more likely
476 that the QMS and BJS pluton share similar magmatic conditions. Using Al^{T} (i.e., Al content on
477 tetrahedral site, which is sensitive to pressure) and $\text{Na} + \text{K}$ (a temperature-sensitive indicator)

478 of amphibole, Chen *et al.* (2018) have shown that most syn-collisional granitoids from the NQO,
479 including both QMS and BJS granitoids, have crystallized under similar conditions at upper
480 crustal pressures of *c.* 200 MPa and temperatures of 785 – 900 °C. Hence, the magmatic
481 crystallization condition is not the cause responsible for the different mineral fractionation in
482 the QMS and BJS plutons. It may also be considered that titanite is likely to be crystallized in
483 relatively oxidized rocks, but this crystallization process is actually accompanied with the
484 stabilisation of other minerals, e.g., the hydration of pyroxene to hornblende ($7 \text{ Hedenbergite} +$
485 $3 \text{ Ilmenite} + 5 \text{ Quartz} + 2 \text{ H}_2\text{O} = 3 \text{ Titanite} + 2 \text{ Fe-Actinolite}$; Frost *et al.*, 2000). However,
486 neither pyroxene nor significant variations of ilmenite/magnetite modal abundances is observed
487 in the QMS granitoids. In addition, there is no clear difference in analyzed LOI contents and
488 hydrous mineral abundances between these two plutons, indicating their similar water/volatile
489 contents. In fact, fractionation of titanite is thus primarily controlled by the melt composition
490 (e.g., Frost *et al.*, 2000; Seifert & Kramer, 2003), e.g., titanite can crystallize only if it is on the
491 liquidus in melt compositions with high Ti and Ca/Al ratios, with high Ca facilitating the
492 stabilisation of titanite (over ilmenite). Both QMS and BJS granitoids are metaluminous,
493 supporting the formation of titanite (e.g., Frost *et al.*, 2000; Seifert & Kramer, 2003; Prowatke
494 and Klemme, 2003), yet titanite is only found in the QMS granitoids. Considering Ti is the
495 requisite major component for titanite (CaTiSiO_5), the crystallization of titanite in the QMS
496 granitoids is thus most likely caused by the higher TiO_2 content of the parental melt, which is
497 inherited from the source. This is also consistent with the noticeably higher TiO_2 content of the
498 QMS granitoids than the BJS granitoids (e.g., 0.97 wt.% in averaged QMS MMEs composition
499 vs. 0.65 wt.% in averaged BJS MMEs composition). The high TiO_2 content in parental magmas

500 facilitated the formation of titanite, the fractionation of which then further controlled the trace
501 element (REE, Y, Nb, Ta and others) systematics in the residual melts towards an adakitic
502 signature.

503 Considering the highly variable composition of melts caused by the partial melting of the
504 subducting/subducted ocean crust with varied compositions (e.g., Niu & Batiza, 1997), the
505 ultimate control is the parental magma composition (major, minor and trace elements), which
506 determines the mineralogy, phase equilibria and trace element behavior during magma
507 evolution. Magmas parental to the QMS pluton with high TiO₂ content and Sr/Y and La/Yb
508 ratios will finally evolve to melts with adakitic signatures after the titanite fractionation,
509 whereas the non-adakitic compositions of the BJS granitoids may be attributed to lower Sr/Y
510 and La/Yb ratios of their parental magmas and the absence of titanite as a result of low TiO₂
511 content. Therefore, parental magmas with high TiO₂ content, high Sr/Y and La/Yb ratios and
512 their further fractionation of titanite due to this original composition, are important
513 characteristics of magmas evolving towards adakitic compositions, as represented by the QMS
514 host granitoids. The potential role of parental magma compositional variation as a result of
515 source compositional variation and the subsequent magma evolution in generating adakitic
516 signature proposed here offer a new insight towards better understanding the widely debated
517 petrogenesis of adakitic rocks.

518 **CONCLUSIONS**

519 In this study, we report major and trace element data on minerals from two well-
520 characterized syn-collisional granitoid plutons in the NQO on the northern margin of the
521 Tibetan plateau to understand the petrogenesis of syn-collisional granitoids with MMEs, which

522 allows us to test the hypothesis that continental collision zones are primary sites for net
523 continental crustal growth.

524 (1) Different trace element budgets in syn-collisional granitoids are systematically
525 identified, and this forms the basis for understanding the effects of mineral fractionation on the
526 compositional variation of the residual melt.

527 (2) Mineral chemistry further testifies that for both QMS and BJS plutons, MMEs are
528 cumulates produced by earlier crystallization of the primitive andesitic melts, which originated
529 from partial melting of subducting/subducted oceanic crust, whereas their host rocks represent
530 the more evolved melt. Given that these syn-collisional granitoids represent juvenile continental
531 crust, our studies support the hypothesis that continental collision zones are primary sites for
532 net continental crust growth by partial melting of the subducted oceanic crust.

533 (3) The mineral compositional differences between QMS and BJS plutons indicate
534 compositionally different parental magmas, corroborated by different compositions of the
535 calculated melts in equilibrium with amphibole. We propose that parental magma composition
536 with high TiO_2 content and high Sr/Y and La/Yb ratios exert a primary control on the formation
537 of adakite and adakitic rocks as in the case of the QMS host granitoids. Among other factors,
538 parental magma compositional variations due to magma source compositional variations
539 control the mineralogy, mineral chemistry and trace element behavior during subsequent
540 magmatic evolution.

541 **ACKNOWLEDGEMENTS**

542 This study was supported by the National Natural Science Foundation of China (Grant numbers:
543 41776096 and 41572047 to Yuanyuan Xiao; U16064101, 41130314 and 41630968 to Yaoling Niu),

544 Laboratory for Marine Geology, Qingdao National Laboratory for Marine Science and Technology, China,
545 and the Excellent Young Project of Institute of Oceanology, Chinese Academy of Sciences (Y52221101Q) to
546 Yuanyuan Xiao. We thank editor Georg Zellmer, and Xiaolong Huang and two anonymous reviewers for
547 constructive comments on an earlier version of this script, which have helped improve the presentation and
548 clarity of this paper.

549 REFERENCES

- 550 Adam, J. & Green, T. H. (1994). The effects of pressure and temperature on the partitioning of
551 Ti, Sr and REE between amphibole, clinopyroxene and basanitic melts. *Chemical*
552 *Geology* 117, 219-233.
- 553 Alonso-Perez, R., Müntener, O. & Ulmer, P. (2009). Igneous garnet and amphibole fractionation
554 in the roots of island arcs: experimental constraints on andesitic liquids. *Contributions*
555 *to Mineralogy and Petrology* 157, 541.
- 556 Barbarin, B. (2005). Mafic magmatic enclaves and mafic rocks associated with some granitoids
557 of the central Sierra Nevada batholith, California: nature, origin, and relations with the
558 hosts. *Lithos* 80, 155-177.
- 559 Barbarin, B. & Didier, J. (1992). Genesis and evolution of mafic microgranular enclaves
560 through various types of interaction between coexisting felsic and mafic magmas. *Earth*
561 *and Environmental Science Transactions of the Royal Society of Edinburgh* 83, 145-153.
- 562 Belousova, E., Griffin, W., O'Reilly, S. Y. & Fisher, N. (2002a). Igneous zircon: trace element
563 composition as an indicator of source rock type. *Contributions to Mineralogy and*
564 *Petrology* 143, 602-622.
- 565 Belousova, E. A., Griffin, W. L., O'Reilly, S. Y. & Fisher, N. I. (2002b). Apatite as an indicator
566 mineral for mineral exploration: trace-element compositions and their relationship to
567 host rock type. *Journal of Geochemical Exploration* 76, 45-69.
- 568 Bottazzi, P., Tiepolo, M., Vannucci, R., Zanetti, A., Brumm, R., Foley, S. F. & Oberti, R. (1999).
569 Distinct site preferences for heavy and light REE in amphibole and the prediction of
570 Amph/LDREE. *Contributions to Mineralogy and Petrology* 137, 36-45.
- 571 Browne, B. L., Eichelberger, J. C., Patino, L. C., Vogel, T. A., Uto, K. & Hoshizumi, H. (2006).
572 Magma mingling as indicated by texture and Sr / Ba ratios of plagioclase phenocrysts
573 from Unzen volcano, SW Japan. *Journal of Volcanology and Geothermal Research* 154,
574 103-116.
- 575 Bruand, E., Storey, C. & Fowler, M. (2014). Accessory Mineral Chemistry of High Ba–Sr
576 Granites from Northern Scotland: Constraints on Petrogenesis and Records of Whole-
577 rock Signature. *Journal of Petrology* 55, 1619-1651.
- 578 Carmichael, I. S. (2002). The andesite aqueduct: perspectives on the evolution of intermediate
579 magmatism in west-central (105–99°W) Mexico. *Contributions to Mineralogy and*
580 *Petrology* 143, 641-663.
- 581 Castillo, P. R. (2012). Adakite petrogenesis. *Lithos* 134–135, 304-316.

- 582 Castillo, P. R., Janney, P. E. & Solidum, R. U. (1999). Petrology and geochemistry of Camiguin
583 Island, southern Philippines: insights to the source of adakites and other lavas in a
584 complex arc setting. *Contributions to Mineralogy and Petrology* 134, 33-51.
- 585 Chambeftort, I., Dilles, J. H. & Longo, A. A. (2013). Amphibole Geochemistry of the Yanacocha
586 Volcanics, Peru: Evidence for Diverse Sources of Magmatic Volatiles Related to Gold
587 Ores. *Journal of Petrology* 54, 1017-1046.
- 588 Chappell, B. W. (1996). Magma Mixing and the Production of Compositional Variation within
589 Granite Suites: Evidence from the Granites of Southeastern Australia. *Journal of*
590 *Petrology* 37, 449-470.
- 591 Chappell, B. W., White, A. J. R. & Wyborn, D. (1987). The Importance of Residual Source
592 Material (Restite) in Granite Petrogenesis. *Journal of Petrology* 28, 1111-1138.
- 593 Chen, B., Chen, Z. C. & Jahn, B. M. (2009). Origin of mafic enclaves from the Taihang
594 Mesozoic orogen, north China craton. *Lithos* 110, 343-358.
- 595 Chen, B., Jahn, B.-M. & Suzuki, K. (2013). Petrological and Nd-Sr-Os isotopic constraints on
596 the origin of high-Mg adakitic rocks from the North China Craton: Tectonic implications.
597 *Geology* 41, 91-94.
- 598 Chen, S., Niu, Y., Li, J., Sun, W., Zhang, Y., Hu, Y. & Shao, F. (2016). Syn-collisional adakitic
599 granodiorites formed by fractional crystallization: Insights from their enclosed mafic
600 magmatic enclaves (MMEs) in the Qumushan pluton, North Qilian Orogen at the
601 northern margin of the Tibetan Plateau. *Lithos* 248–251, 455-468.
- 602 Chen, S., Niu, Y., Sun, W., Zhang, Y., Li, J., Guo, P. & Sun, P. (2015). On the origin of mafic
603 magmatic enclaves (MMEs) in syn-collisional granitoids: evidence from the Baojishan
604 pluton in the North Qilian Orogen, China. *Mineralogy and Petrology* 109, 577-596.
- 605 Chen, S., Niu, Y. & Xue, Q. (2018). Syn-collisional felsic magmatism and continental crust
606 growth: A case study from the North Qilian Orogenic Belt at the northern margin of the
607 Tibetan Plateau. *Lithos* 308-309, 53-64.
- 608 Chung, S.-L., Liu, D., Ji, J., Chu, M.-F., Lee, H.-Y., Wen, D.-J., Lo, C.-H., Lee, T.-Y., Qian, Q.
609 & Zhang, Q. (2003). Adakites from continental collision zones: Melting of thickened
610 lower crust beneath southern Tibet. *Geology* 31, 1021-1024.
- 611 Condie, K.C. (1998). Episodic continental growth and supercontinents. *Earth and Planetary*
612 *Science Letters* 163, 97-108.
- 613 Dahlquist, J.A. (2002). Mafic microgranular enclaves: early segregation from metaluminous
614 magma (Sierra de Chepes), Pampean Ranges, NW Argentina. *Journal of South*
615 *American Earth Sciences* 15: 643-655.
- 616 Defant, M. J. & Drummond, M. S. (1990). Derivation of some modern arc magmas by melting
617 of young subducted lithosphere. *Nature* 347, 662-665.
- 618 Frost, B. R., Chamberlain, K. R. & Schumacher, J. C. (2000). Sphene (titanite): phase relations
619 and role as a geochronometer. *Chemical Geology* 172, 131-148.
- 620 Gao, S., Rudnick, R. L., Yuan, H.-L., Liu, X.-M., Liu, Y.-S., Xu, W.-L., Ling, W.-L., Ayers, J.,
621 Wang, X.-C. & Wang, Q.-H. (2004). Recycling lower continental crust in the North
622 China craton. *Nature* 432, 892-897.
- 623 Green, T.H., Adam, J. & Site, S.H. (1993). Proton microprobe determined trace element
624 partition coefficients between pargasite, augite and silicate or carbonatitic melts. EOS,
625 *Transactions of the American Geophysical Union* 74: 340.

- 626 Hidalgo, P. J. & Rooney, T. O. (2010). Crystal fractionation processes at Baru volcano from the
627 deep to shallow crust. *Geochemistry, Geophysics, Geosystems* 11, n/a-n/a.
- 628 Hidalgo, S., Monzier, M., Martin, H., Chazot, G., Eissen, J.-P. & Cotten, J. (2007). Adakitic
629 magmas in the Ecuadorian Volcanic Front: Petrogenesis of the Iliniza Volcanic Complex
630 (Ecuador). *Journal of Volcanology and Geothermal Research* 159, 366-392.
- 631 Hofmann, A. W. (1988). Chemical differentiation of the Earth: the relationship between mantle,
632 continental crust, and oceanic crust. *Earth and Planetary Science Letters* 90, 297-314.
- 633 Hoskin, P. W. O. & Schaltegger, U. (2003). The Composition of Zircon and Igneous and
634 Metamorphic Petrogenesis. *Reviews in mineralogy and geochemistry* 53, 27-62.
- 635 Huang, H., Niu, Y. & Mo, X. (2016). Syn-collisional granitoids in the Qilian Block on the
636 Northern Tibetan Plateau: A long-lasting magmatism since continental collision through
637 slab steepening. *Lithos* 246–247, 99-109.
- 638 Huang, H., Niu, Y., Nowell, G., Zhao, Z., Yu, X., Zhu, D.-C., Mo, X. & Ding, S. (2014).
639 Geochemical constraints on the petrogenesis of granitoids in the East Kunlun Orogenic
640 belt, northern Tibetan Plateau: Implications for continental crust growth through syn-
641 collisional felsic magmatism. *Chemical Geology* 370, 1-18.
- 642 Huang, H., Niu, Y. & Mo, X. (2017). Garnet effect on Nd-Hf isotope decoupling: Evidence
643 from the Jinfosi batholith, Northern Tibetan Plateau. *Lithos* 274-275, 31-38.
- 644 Huang, H., Niu, Y., Nowell, G., Zhao, Z., Yu, X., Mo, X. & Ding, S. (2015). The nature and
645 history of the Qilian Block in the context of the development of the Greater Tibetan
646 Plateau. *Gondwana Research* 28, 209-224.
- 647 Jochum, K. P., Willbold, M., Raczek, I., Stoll, B. & Herwig, K. (2005). Chemical
648 characterisation of the USGS reference glasses GSA-1G, GSC-1G, GSD-1G, GSE-1G,
649 BCR-2G, BHVO-2G and BIR-1G using EPMA, ID-TIMS, ID-ICP-MS and LA-ICP-
650 MS. *Geostandards and Geoanalytical Research* 29, 285-302.
- 651 Klein, M., Stosch, H. G. & Seck, H. A. (1997). Partitioning of high field-strength and rare-earth
652 elements between amphibole and quartz-dioritic to tonalitic melts: an experimental
653 study. *Chemical Geology* 138, 257-271.
- 654 Lin, J., Liu, Y., Yang, Y. & Hu, Z. (2016). Calibration and correction of LA-ICP-MS and LA-
655 MC-ICP-MS analyses for element contents and isotopic ratios. *Solid Earth Sciences* 1,
656 5-27.
- 657 Liu, L., Qiu, J.-S. & Li, Z. (2013). Origin of mafic microgranular enclaves (MMEs) and their
658 host quartz monzonites from the Muchen pluton in Zhejiang Province, Southeast China:
659 Implications for magma mixing and crust–mantle interaction. *Lithos* 160–161, 145-163.
- 660 Liu, Y., Hu, Z., Gao, S., Günther, D., Xu, J., Gao, C. & Chen, H. (2008). In situ analysis of
661 major and trace elements of anhydrous minerals by LA-ICP-MS without applying an
662 internal standard. *Chemical Geology* 257, 34-43.
- 663 Macpherson, C. G., Dreher, S. T. & Thirlwall, M. F. (2006). Adakites without slab melting:
664 high pressure differentiation of island arc magma, Mindanao, the Philippines. *Earth and
665 Planetary Science Letters* 243, 581-593.
- 666 Marks, M. A. W., Coulson, I. M., Schilling, J., Jacob, D. E., Schmitt, A. K. & Markl, G. (2008).
667 The effect of titanite and other HFSE-rich mineral (Ti-bearing andradite, zircon,
668 eudialyte) fractionation on the geochemical evolution of silicate melts. *Chemical
669 Geology* 257, 153-172.

- 670 Matsui, Y. (1977). Crystal structure control in trace element partition between crystal and
671 magma. *Tectonics* 100, 315-324.
- 672 McLeod, G. W., Dempster, T. J. & Faithfull, J. W. (2011). Deciphering Magma-Mixing
673 Processes Using Zoned Titanite from the Ross of Mull Granite, Scotland. *Journal of*
674 *Petrology* 52, 55-82.
- 675 Mo, X., Niu, Y., Dong, G., Zhao, Z., Hou, Z., Zhou, S. & Ke, S. (2008). Contribution of
676 syncollisional felsic magmatism to continental crust growth: A case study of the
677 Paleogene Linzizong volcanic Succession in southern Tibet. *Chemical Geology* 250, 49-
678 67.
- 679 Niu, Y. L. (2005). Generation and evolution of basaltic magmas: some basic concepts and a
680 new view on the origin of Mesozoic-Cenozoic basaltic volcanism in Eastern China.
681 *Geological Journal of China University* 11, 9-46.
- 682 Niu, Y. L. & Batiza, R. (1997). Trace element evidence from seamounts for recycled oceanic
683 crust in the Eastern Pacific mantle. *Earth and Planetary Science Letters* 148, 471-483.
- 684 Niu, Y., Mo, X., Dong, G., Zhao, Z., Hou, Z. Zhou, S. & Ke, S. (2007). Continental Collision
685 Zones are Primary Sites of net Continental Crustal Growth: Evidence From the
686 Linzizong Volcanic Succession in Southern Tibet. *Eos Trans. AGU* 88(52), Fall Meet.,
687 Suppl., Abstract V34A-01.
- 688 Niu, Y. L. & O'Hara, M. J. (2009). MORB mantle hosts the missing Eu (Sr, Nb, Ta and Ti) in
689 the continental crust: New perspectives on crustal growth, crust-mantle differentiation
690 and chemical structure of oceanic upper mantle. *Lithos* 112, 1-17.
- 691 Niu, Y., Zhao, Z., Zhu, D.-C. & Mo, X. (2013). Continental collision zones are primary sites
692 for net continental crust growth — A testable hypothesis. *Earth-Science Reviews* 127,
693 96-110.
- 694 O' Nions, R. K., Evensen, N. M. & Hamilton, P. J. (1979). Geochemical modelling of mantle
695 differentiation and crustal growth. *Journal of Geophysical Research* 84, 6091-6101.
- 696 Piccoli, P., Candela, P. & Rivers, M. (2011). Interpreting magmatic processes from accessory
697 phases: titanite—a small-scale recorder of large-scale processes. *Earth and*
698 *Environmental Science Transactions of the Royal Society of Edinburgh* 91, 257-267.
- 699 Ribeiro, J. M., Maury, R. C. & Grégoire, M. (2016). Are Adakites Slab Melts or High-pressure
700 Fractionated Mantle Melts? *Journal of Petrology* 57, 839-862.
- 701 Richards, J. P. & Kerrich, R. (2007). Special Paper: Adakite-Like Rocks: Their Diverse Origins
702 and Questionable Role in Metallogenesis. *Economic Geology* 102, 537-576.
- 703 Rodríguez, C., Sellés, D., Dungan, M., Langmuir, C. & Leeman, W. (2007). Adakitic Dacites
704 Formed by Intracrustal Crystal Fractionation of Water-rich Parent Magmas at Nevado
705 de Longaví Volcano (36·2°S; Andean Southern Volcanic Zone, Central Chile). *Journal*
706 *of Petrology* 48, 2033-2061.
- 707 Rooney, T. O., Franceschi, P. & Hall, C. M. (2011). Water-saturated magmas in the Panama
708 Canal region: a precursor to adakite-like magma generation? *Contributions to*
709 *Mineralogy and Petrology* 161, 373-388.
- 710 Seifert, W. & Kramer, W. (2003). Accessory titanite: an important carrier of zirconium in
711 lamprophyres. *Lithos* 71, 81-98.
- 712 Sha, L.-K. & Chappell, B. W. (1999). Apatite chemical composition, determined by electron
713 microprobe and laser-ablation inductively coupled plasma mass spectrometry, as a

- 714 probe into granite petrogenesis. *Geochimica et Cosmochimica Acta* 63, 3861-3881.
- 715 Smith, M. P., Storey, C. D., Jeffries, T. E. & Ryan, C. (2009). In Situ U–Pb and Trace Element
716 Analysis of Accessory Minerals in the Kiruna District, Norrbotten, Sweden: New
717 Constraints on the Timing and Origin of Mineralization. *Journal of Petrology* 50, 2063-
718 2094.
- 719 Song, S., Niu, Y., Su, L., Wei, C. & Zhang, L. (2014a). Adakitic (tonalitic-trondhjemitic)
720 magmas resulting from eclogite decompression and dehydration melting during
721 exhumation in response to continental collision. *Geochimica et Cosmochimica Acta* 130,
722 42-62.
- 723 Song, S., Niu, Y., Su, L. & Xia, X. (2013). Tectonics of the North Qilian orogen, NW China.
724 *Gondwana Research* 23, 1378-1401.
- 725 Song, S., Niu, Y., Su, L., Zhang, C. & Zhang, L. (2014b). Continental orogenesis from ocean
726 subduction, continent collision/subduction, to orogen collapse, and orogen recycling:
727 The example of the North Qaidam UHPM belt, NW China. *Earth-Science Reviews* 129,
728 59-84.
- 729 Song, S., Niu, Y., Zhang, L. & Zhang, G. (2009). Time constraints on orogenesis from oceanic
730 subduction to continental subduction, collision, and exhumation: An example from
731 North Qilian and North Qaidam HP-UHP belts. *Acta Petrologica Sinica* 25, 2067-2077.
- 732 Song, S., Zhang, L., Niu, Y., Su, L., Song, B. & Liu, D. (2006). Evolution from oceanic
733 subduction to continental collision: A case study from the Northern Tibetan Plateau
734 based on geochemical and geochronological data. *Journal of Petrology* 47, 435-455.
- 735 Stern, R. J. & Scholl, D. W. (2010). Yin and yang of continental crust creation and destruction
736 by plate tectonic processes. *International Geology Review* 52, 1-31.
- 737 Streck, M. J., Leeman, W. P. & Chesley, J. (2007). High-magnesian andesite from Mount Shasta:
738 A product of magma mixing and contamination, not a primitive mantle melt. *Geology*
739 35, 351-354.
- 740 Sun, S.-s. & McDonough, W. F. (1989). Chemical and isotopic systematics of oceanic basalts:
741 implications for mantle composition and processes. *Geological Society, London, Special*
742 *Publications* 42, 313-345.
- 743 Tang, G.-J., Wang, Q., Wyman, D. A., Chung, S.-L., Chen, H.-Y. & Zhao, Z.-H. (2017). Genesis
744 of pristine adakitic magmas by lower crustal melting: A perspective from amphibole
745 composition. *Journal of Geophysical Research: Solid Earth* 122, 1934-1948.
- 746 Taylor, S.R. (1967). The origin and growth of continents. *Tectonophysics* 4, 17 - 34.
- 747 Taylor S R. (1977). Island arc models and the composition of the continental crust. In: Talwani
748 M, Pitman W C III, eds. *Island Arcs, Deep Sea Trenches, and Back-Arc Basins*. Am
749 Geophys Union, Maurice Ewing Ser, 1: 325-335
- 750 Tiepolo, M., Langone, A., Morishita, T. & Yuhara, M. (2012). On the Recycling of Amphibole-
751 rich Ultramafic Intrusive Rocks in the Arc Crust: Evidence from Shikanoshima Island
752 (Kyushu, Japan). *Journal of Petrology* 53, 1255-1285.
- 753 Tiepolo, M., Oberti, R. & Vannucci, R. (2002). Trace-element incorporation in titanite:
754 constraints from experimentally determined solid/liquid partition coefficients. *Chemical*
755 *Geology* 191, 105-119.
- 756 Tseng, C.-Y., Yang, H.-J., Yang, H.-Y., Liu, D., Wu, C., Cheng, C.-K., Chen, C.-H. & Ker, C.-
757 M. (2009). Continuity of the North Qilian and North Qinling orogenic belts, Central

- 758 Orogenic System of China: Evidence from newly discovered Paleozoic adakitic rocks.
759 *Gondwana Research* 16, 285-293.
- 760 Wang, Q., McDermott, F., Xu, J.-f., Bellon, H. & Zhu, Y.-t. (2005). Cenozoic K-rich adakitic
761 volcanic rocks in the Hohxil area, northern Tibet: Lower-crustal melting in an
762 intracontinental setting. *Geology* 33, 465-468.
- 763 Wang, Q., Wyman, D. A., Xu, J., Jian, P., Zhao, Z., Li, C., Xu, W., Ma, J. & He, B. (2007).
764 Early Cretaceous adakitic granites in the Northern Dabie Complex, central China:
765 Implications for partial melting and delamination of thickened lower crust. *Geochimica
766 et Cosmochimica Acta* 71, 2609-2636.
- 767 Xia, L. Q., Xia, Z. C. & Xu, X. Y. (2003). Magmatogenesis in the Ordovician backarc basins of
768 the northern Qilian Mountains, China. *Geological Society of America Bulletin* 115,
769 1510-1522.
- 770 Xia, X., Song, S. & Niu, Y. (2012). Tholeiite–Boninite terrane in the North Qilian suture zone:
771 Implications for subduction initiation and back-arc basin development. *Chemical
772 Geology* 328, 259-277.
- 773 Xia, X. H. & Song, S. G. (2010). Forming age and tectono-petrogeneses of the Jiugequan
774 ophiolite in the North Qilian Mountain, NW China. *Chinese Science Bulletin* 55, 1899-
775 1907.
- 776 Xiao, Y., Niu, Y., Song, S., Davidson, J. & Liu, X. (2013). Elemental responses to subduction-
777 zone metamorphism: Constraints from the North Qilian Mountain, NW China. *Lithos*
778 160–161, 55-67.
- 779 Yu, S., Zhang, J., Qin, H., Sun, D., Zhao, X., Cong, F. & Li, Y. (2015). Petrogenesis of the early
780 Paleozoic low-Mg and high-Mg adakitic rocks in the North Qilian orogenic belt, NW
781 China: Implications for transition from crustal thickening to extension thinning. *Journal
782 of Asian Earth Sciences* 107, 122-139.
- 783 Zhang, Y., Niu, Y., Hu, Y., Liu, J., Ye, L., Kong, J. & Duan, M. (2016). The syncollisional
784 granitoid magmatism and continental crust growth in the West Kunlun Orogen, China –
785 Evidence from geochronology and geochemistry of the Arkarz pluton. *Lithos* 245, 191-
786 204.
- 787 Zhang, B., Hu, X., Li, P., Tang, Q. & Zhou, W. (2019). Trace element partitioning between
788 amphibole and hydrous silicate glasses at 0.6-2.6 GPa. *Acta Geochim* 38, 414-429.

789 SUPPLEMENTARY MATERIALS

790 Supplementary data can be found in the online version of this article:

791 **Table DR1** Average bulk-rock compositions for MMEs and hosts from the BJS and QMS
792 plutons in the eastern NQO (Chen *et al.*, 2015, 2016)

793 **Table DR2** Operation conditions of LA-ICP-MS for analysis of mineral compositions in
794 this study

795 **Table DR3** Analytical results of amphibole in the BJS and QMS plutons using LA-ICP-
796 MS

797 **Table DR4** Analytical results of biotite and muscovite in the BJS and QMS plutons using
798 LA-ICP-MS

799 **Table DR5** Analytical results of plagioclase and orthoclase in the BJS and QMS plutons
800 using LA-ICP-MS

801 **Table DR6** Analytical results of apatite in the BJS and QMS plutons using LA-ICP-MS

802 **Table DR7** Analytical results of epidote in the BJS and QMS plutons using LA-ICP-MS

803 **Table DR8** Analytical results of titanite in the BJS and QMS plutons using LA-ICP-MS

804 **Table DR9** Analytical results of carbonate and zircon in the BJS and QMS plutons using
805 LA-ICP-MS

806 **Table DR10** Analytical results of zircon by Chen *et al.* (2015, 2016) in the BJS and QMS
807 plutons using LA-ICP-MS

808 **Table DR11** Modelling mineral weight proportions and chemical element budgets in
809 MMEs and host rocks of the QMS and BJS plutons

810 **Table DR12** Partition coefficients for several selected mineral pairs in our studied rocks

811 **Table DR13** Calculated compositions of the melts in equilibrium with amphibole and
812 partition coefficients between amphibole and melts used in this study.

813 **Fig. DR1** Analytical accuracy (RE in %; a) and precision (RSD in %; b) of LA-ICP-MS
814 analysis determined by a synthesized reference glass GSE-1G (Jochum *et al.*, 2005) as an
815 unknown sample.

816 **FIGURE CAPTIONS**

817 **Figure 1 (a-b)** Geological map of NQO and sample locations for this study (after Chen *et al.*, 2015, 2016). **(c-d)** Field photos showing the sharp contact between host rocks and MMEs.

819 **Figure 2 (a-h)** Photomicrographs for host granitoids (in the left column, i.e., a,c,e,g) and MMEs (in the right column, i.e., b,d,f,h) in pairs from the BJS and QMS plutons in the eastern NQO. (a-d) are for granitoids from the BJS pluton with more epidote; (e-h) are for granitoids from the QMS pluton with abundant titanite. Mineral abbreviations are: AB – albite, AMP – amphibole, AP – apatite, BT – biotite, EP – epidote, MUS – muscovite, QZ – quartz, TTN – titanite, ZRN – zircon. Primitive mantle values are from Sun & McDonough (1989).

825 **Figure 3 (a)** Primitive mantle (Sun & McDonough, 1989) normalized trace element pattern for average bulk-rock compositions of MMEs and their host rocks from the BJS and QMS plutons (Chen *et al.*, 2015, 2016). **(b-h)** Primitive mantle (Sun & McDonough, 1989) normalized average mineral compositions of MMEs and their host granitoids from the QMS and BJS plutons respectively.

830 **Figure 4 (a-d)** Mg# ($= 100 * \text{Mg} / [\text{Mg} + \text{Fe}^{2+}]$) and Nb/Ta ratio profiles for amphibole in MMEs and their host granitoids from the BJS (a-b) and QMS (c-d) plutons. H – Host, M – MME, AVG – average. Numbers are read as follows, e.g., ⑧ 64.5/29.3 means analytical spot 8 has Mg# = 64.5 and Nb/Ta = 29.3 given in Table DR3. **(e-h)** Elemental and ratio co-variation diagrams for amphibole from the two plutons.

835 **Figure 5 (a-b)** Nb/Ta ratio variation of biotite from the BJS and QMS plutons. Numbers are read as follows, e.g., 8: 15.5 means analytical spot 8 has Nb/Ta = 15.5 given in Table DR4. **(c-d)** Mg# variation diagrams for Al₂O₃ and Nb/Ta ratios of biotite from the two plutons.

838 **Figure 6 (a-d)** Anorthite and Sr content variation for plagioclase in MMEs and their host
839 granitoids from the BJS (a-b) and QMS (c-d) plutons. Numbers are read as follows, e.g., ⑧ or
840 8: 44/723 means analytical spot 8 has An = 44 and Ba = 723 ppm given in Table DR5. **(e-h)**
841 An-variation diagrams for Sr, Ba, La and Y of plagioclase from the two plutons.

842 **Figure 7** Titanite compositional variation for the BJS and QMS plutons. Analytical spot
843 numbers in both left and right panels are as given in Table DR8. The position numbers
844 highlighted in red in the right panels represent those analyzed points with more reddish colour,
845 the element contents of which plot in grey areas as indicated in the right panels. This shows that
846 the more reddish parts tend to have higher Nb-Ta-Zr-Hf-Th-U-Pb-La (LREE)-Lu (HREE).

847 **Figure 8** Elemental and ratio co-variation diagrams for titanite from the QMS pluton. In
848 (e-f), the modelled bulk parental magma composition using the average composition of
849 amphibole in MMEs of the QMS pluton (Sr/Y = 30, La/Yb = 23) is also plotted, for comparison.
850 The extremely low Sr/Y and La/Yb ratios of titanite relative to those of the bulk parental magma
851 indicate that the fractionation of titanite can effectively increase these ratios in the residual melts.

852 **Figure 9** Reconstructed elemental budgets in bulk-rock MMEs and their host rocks from
853 the BJS and QMS plutons, normalized against their average bulk-rock compositions (Table

854 DR1). “% whole rock” = $100\% * \sum_{i=1, j=1}^{i=m, j=n} X_i Y_j / Z_j$, where i refers to different mineral phases, j

855 refers to different chemical elements, X refers to modelled mineral modal proportions (Table

856 DR11), Y refers to average content of chemical element j in analyzed mineral i (Tables DR3-

857 9), Z refers to average content of chemical element j in analyzed bulk-rock samples (Table DR1),

858 as indicated by the red dot-dashed lines in each panel. Bars with different colours represent

859 different mineral hosts.

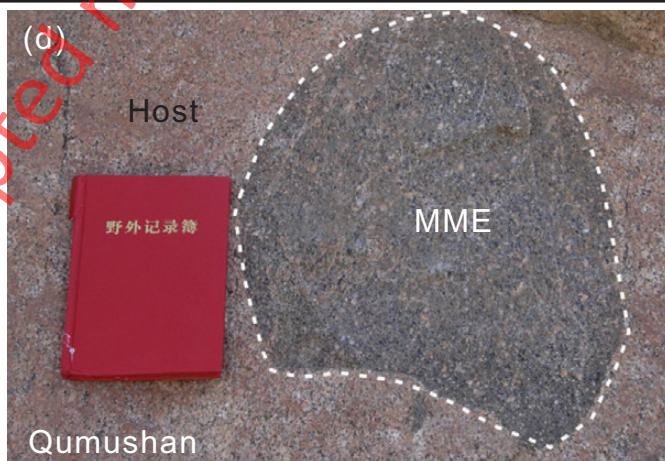
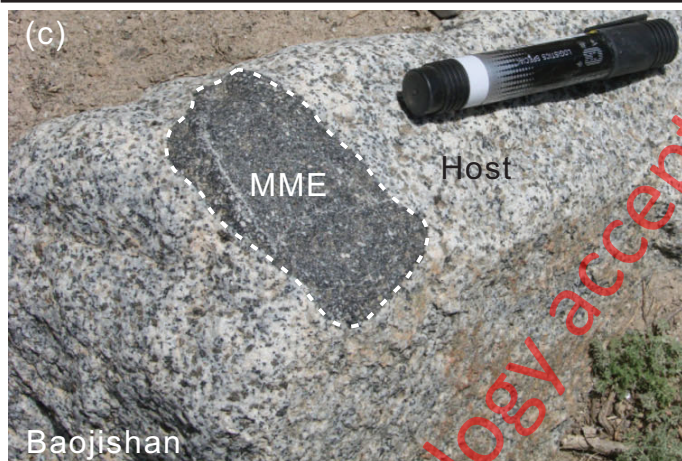
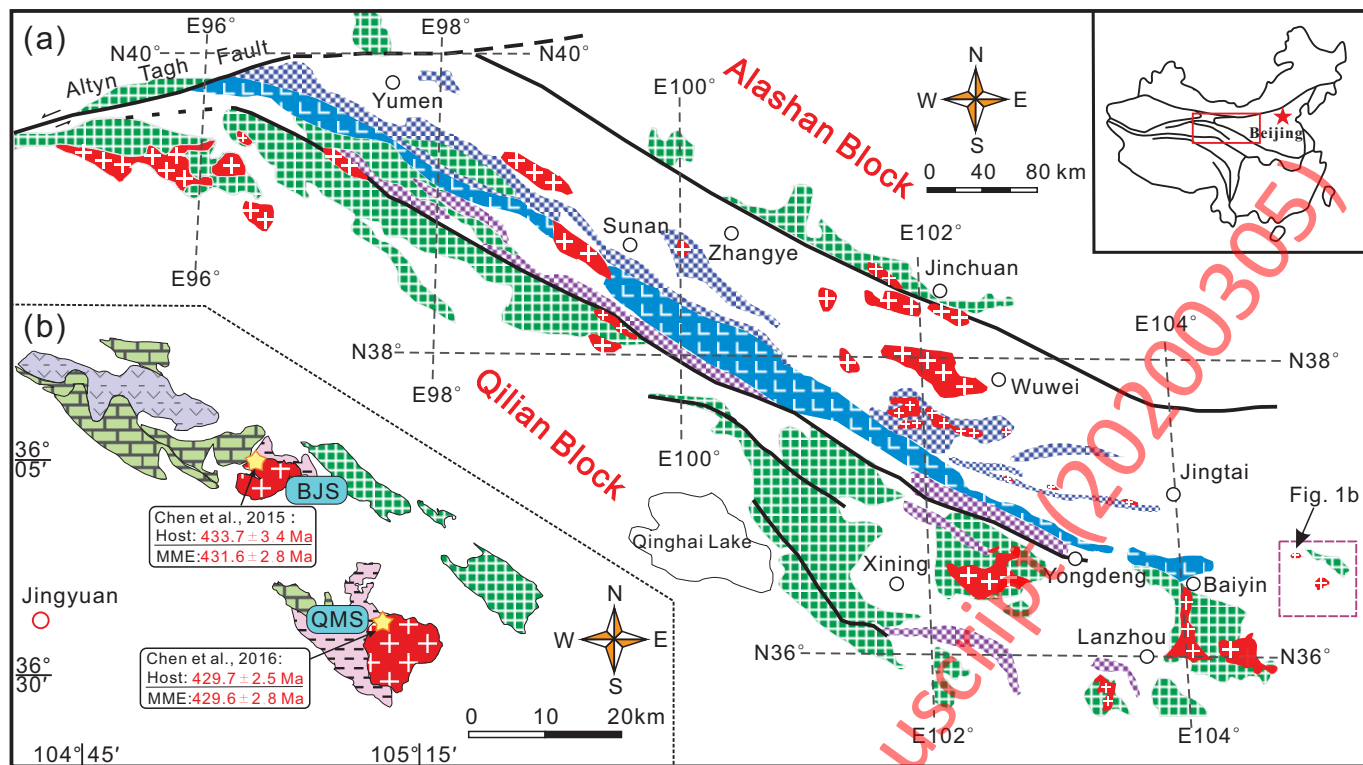
860 **Figure 10** Cartoon illustrating the petrogenesis of MMEs and host rocks. The development
861 of MMEs in the context of the syn-collisional granitoid magma generation and evolution can
862 be generalized in three stages (Niu *et al.*, 2013; Chen *et al.*, 2015, 2016, 2018): Stage I –
863 Compositionally heterogeneous ocean crust plus some terrigenous sediments melt to produce
864 andesitic magmas during the continental collision under amphibolite facies conditions; Stage II
865 – Interaction of such magmas with mantle peridotite during ascent; Stage III – intrusion of the
866 andesitic magmas into the “cold” crust to develop a magma chamber with the rapid cooling
867 resulting in the crystallization of fine-grained cumulate dominated by mafic minerals near the
868 walls and base of the magma chamber to be later dispersed as MMEs in the slowly cooling
869 magma bodies that solidified as the granitoid host. Among other minerals, fractionation of
870 titanite, zircon and amphibole will lead to significant increase in Sr/Y and La/Yb ratios as
871 observed in host rocks, which may lead to the formation of adakitic signatures as displayed by
872 the QMS host rocks. BCC – bulk continent crust.

873 **Figure 11** Co-variation diagrams for Sr/Y vs. Sr and La/Yb vs. La of various minerals in
874 the BJS and QMS plutons. The parental magma composition calculated using the average
875 composition of amphibole in the QMS MMEs (Sr/Y = 30, La/Yb = 23) is also indicated for
876 comparison. Notably, fractionation of those minerals with lower Sr/Y and La/Yb ratios than the
877 bulk parental magma will increase these two ratios in the residual melts.

878 **Figure 12** Primitive mantle (PM; Sun & McDonough, 1989) normalized trace element
879 abundances for calculated compositions of melt in equilibrium with amphibole from MMEs
880 and their host rocks of the BJS and QMS plutons, respectively. The thick black lines are the
881 average bulk rock compositions of MMEs and their host granitoids from the two plutons,

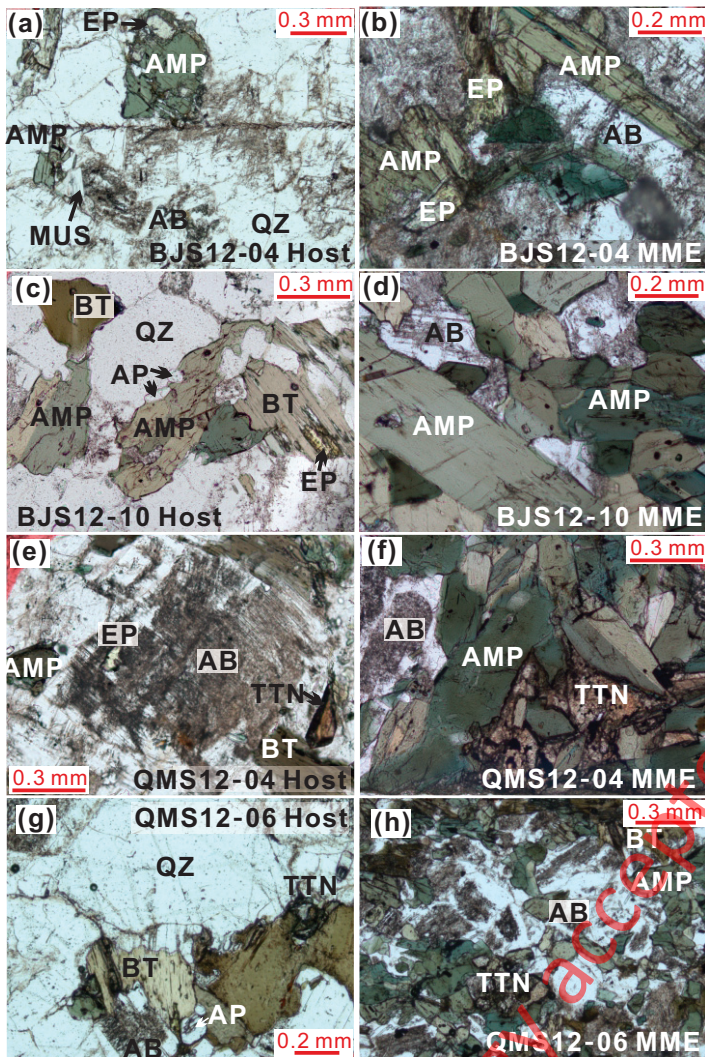
882 respectively. Average mineral compositions in Tables DR3-9 are also plotted to indicate the
883 contribution of various minerals.

884 **Figure 13** Co-variation diagrams of Sr/Y – Y (a), La/Yb – Yb (b) and Eu/Eu* – [La/Yb]_N
885 (c) for melts in equilibrium with amphibole in MMEs of QMS (the red area) and BJS (the grey
886 area) plutons. In (d), the average Sr/Y and La/Yb ratios of different minerals in the QMS MMEs
887 are plotted for comparison, i.e., those lower than the original melt composition (Sr/Y = 30,
888 La/Yb = 23) can effectively increase these two ratios in the residual melts. The original melt
889 composition is calculated by using the average composition of amphibole in the QMS MMEs.
890 (a-c) Also shown are modelling results for the evolution of the original melt initially in
891 equilibrium with MME amphibole in the QMS pluton, assuming mineral modal abundances as
892 in Table DR 11 (25% amphibole + 45% plagioclase + 20% biotite + 1.7% apatite + 0.5% titanite
893 + 2.4% epidote + 0.03% zircon). The insert diagrams in (a-c) show modelling results for the
894 related Rayleigh fractional crystallization of various minerals. The parental magmas of the
895 QMS pluton (the red area) clearly show higher Sr/Y and La/Yb ratios than those of the BJS
896 pluton (the grey area), and are comparable to adakites. The fractionation of amphibole, titanite,
897 and zircon further increases these two ratios and finally form the adakitic characteristics of the
898 QMS host granitoids. The selected partition coefficient values are from Green *et al.* (1993),
899 Hidalgo *et al.* (2007), Matsui (1977) and Klein *et al.* (1997), and are given in Table DR13. The
900 discrimination lines in (a-b) are from Defant & Drummond (1990) and Richards & Kerrich
901 (2007), respectively.



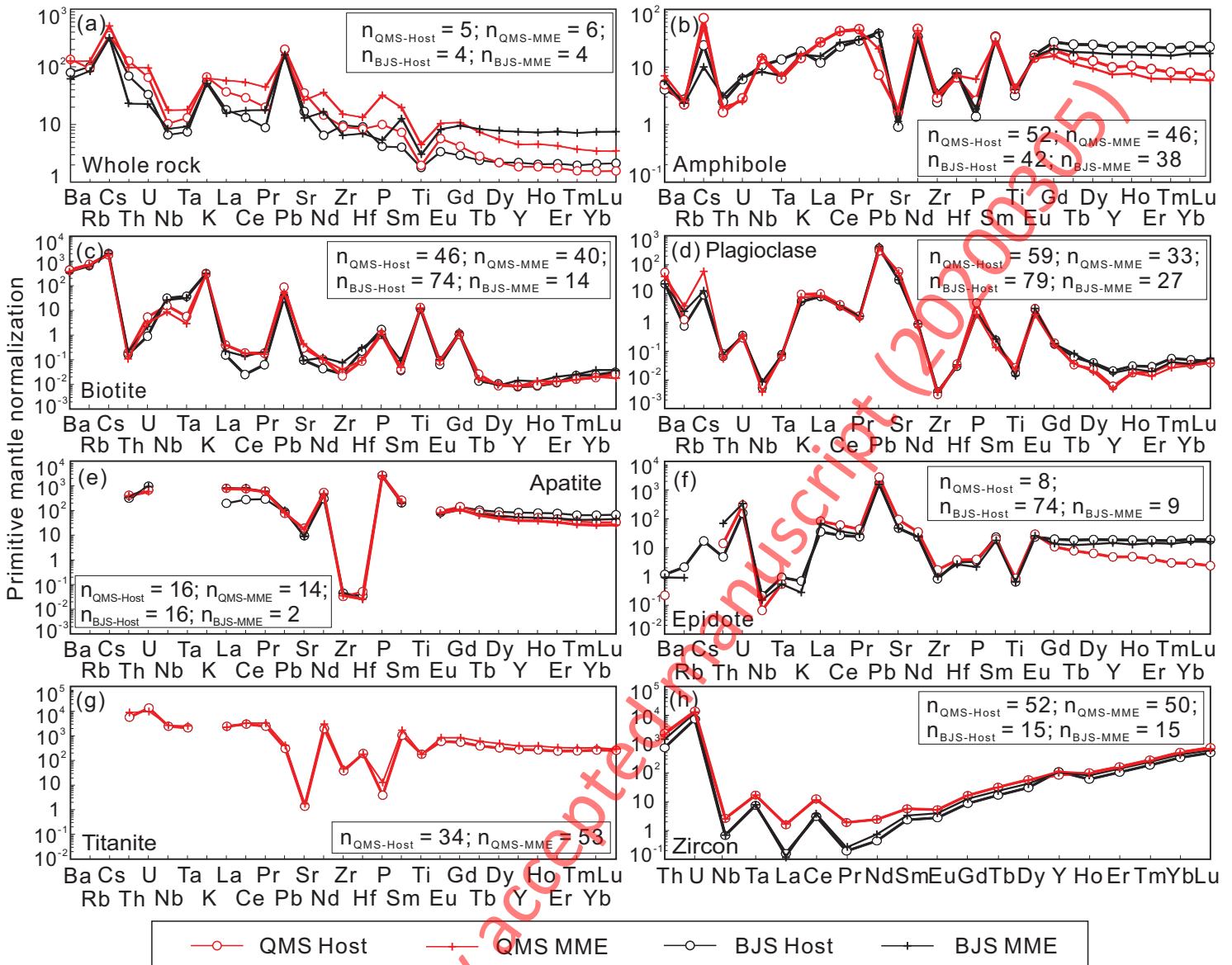
Journal of Petrology accepted manuscript (20200305)

Xiao et al., Fig. 2 Photomicrographs



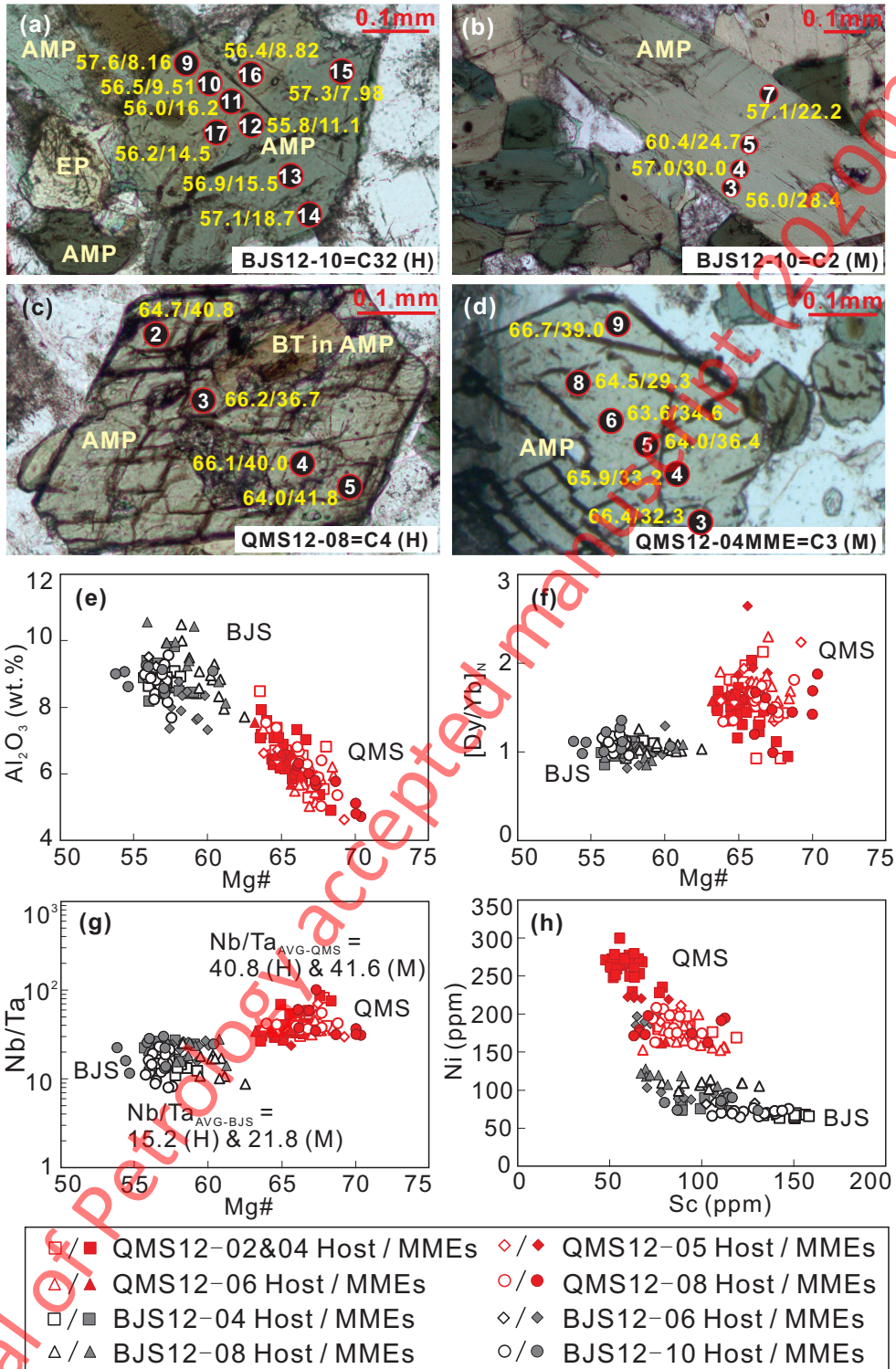
Journal of Petrology (20200305)

Xiao et al, Fig. 3 PM normalized trace element distributed patterns of averaged bulk-rock composition and different minerals

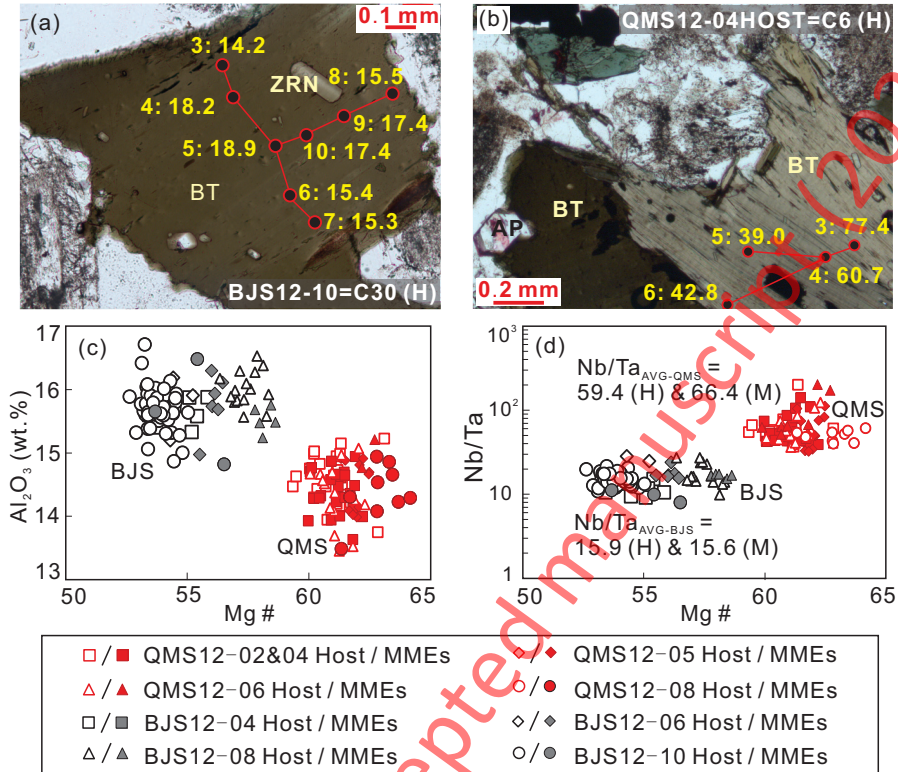


Journal of Petrology

Xiao et al., Fig. 4 Mg# and Nb/Ta profiles in amphibole

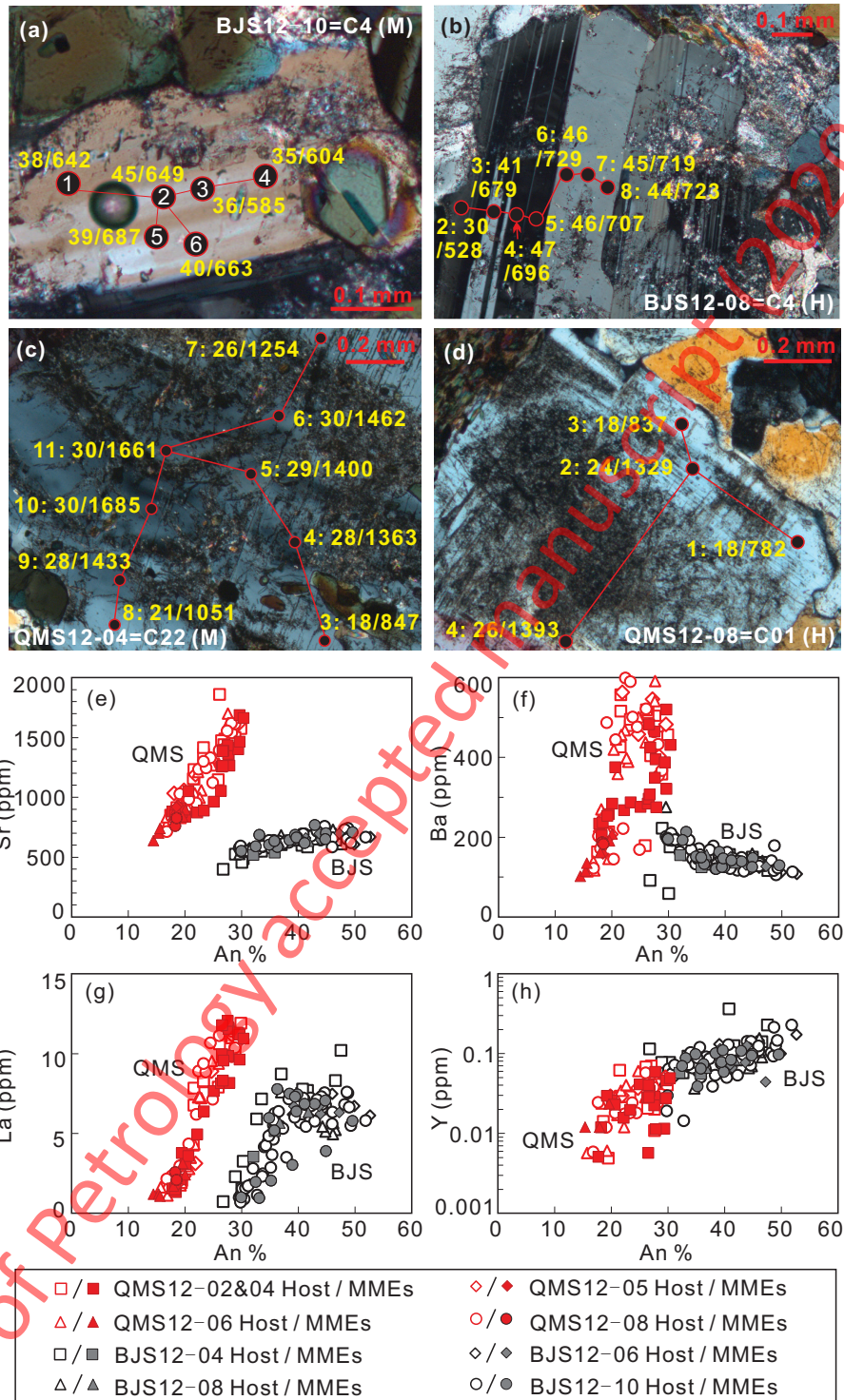


Xiao et al., Fig. 5 Nb/Ta profiles of biotite

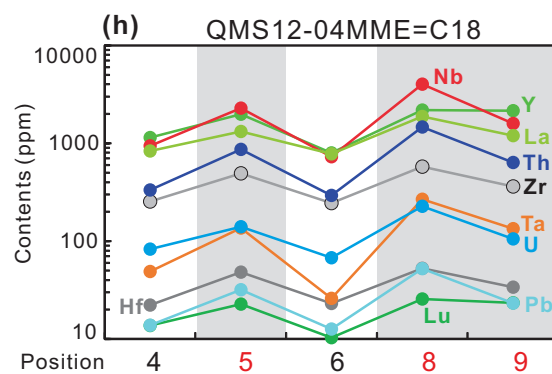
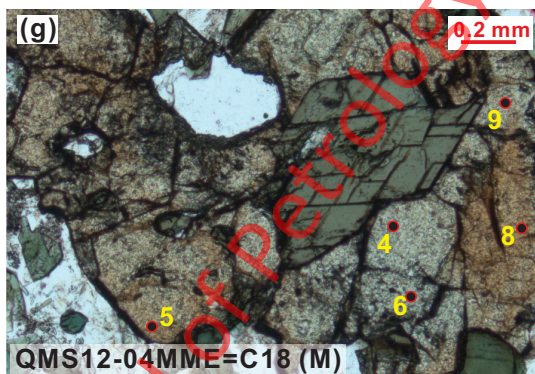
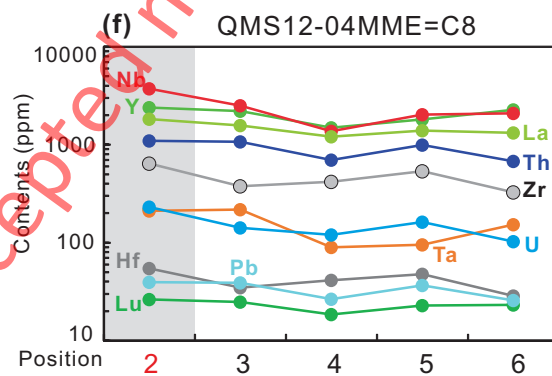
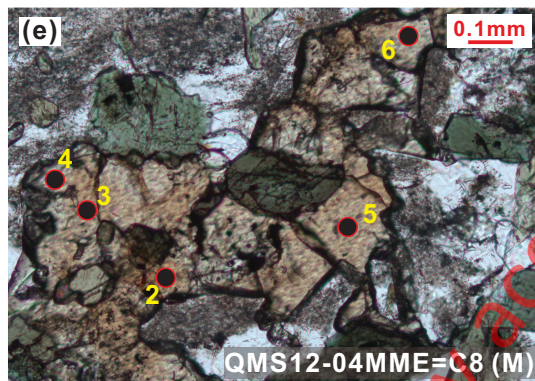
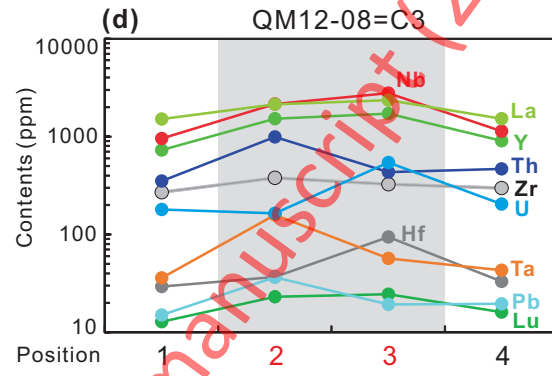
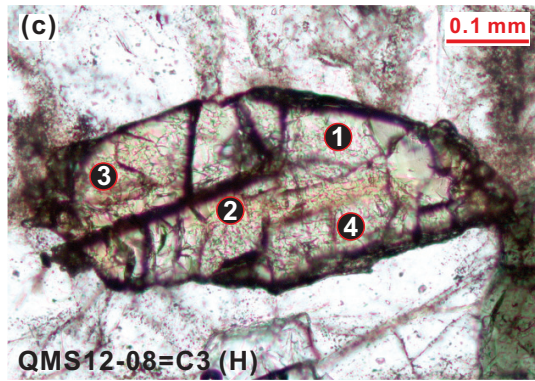
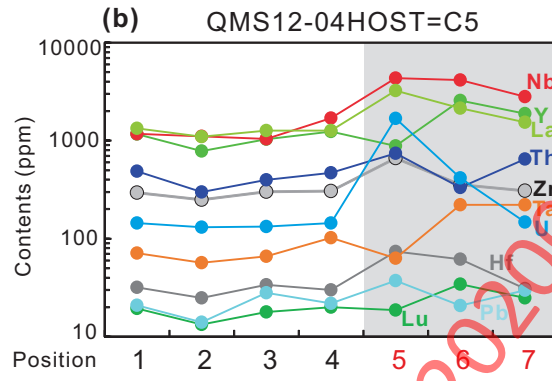
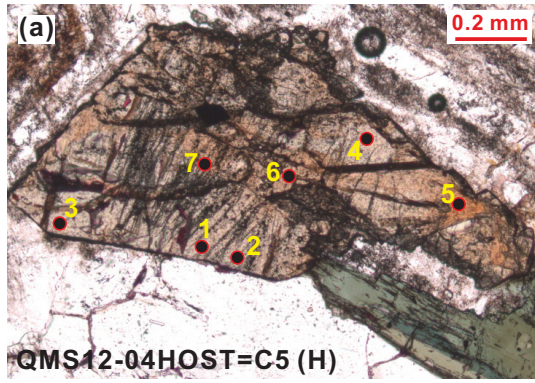


Journal of Petrology accepted manuscript (20200305)

Xiao et al., Fig.6 Anorthite profile and Sr contents of plagioclase

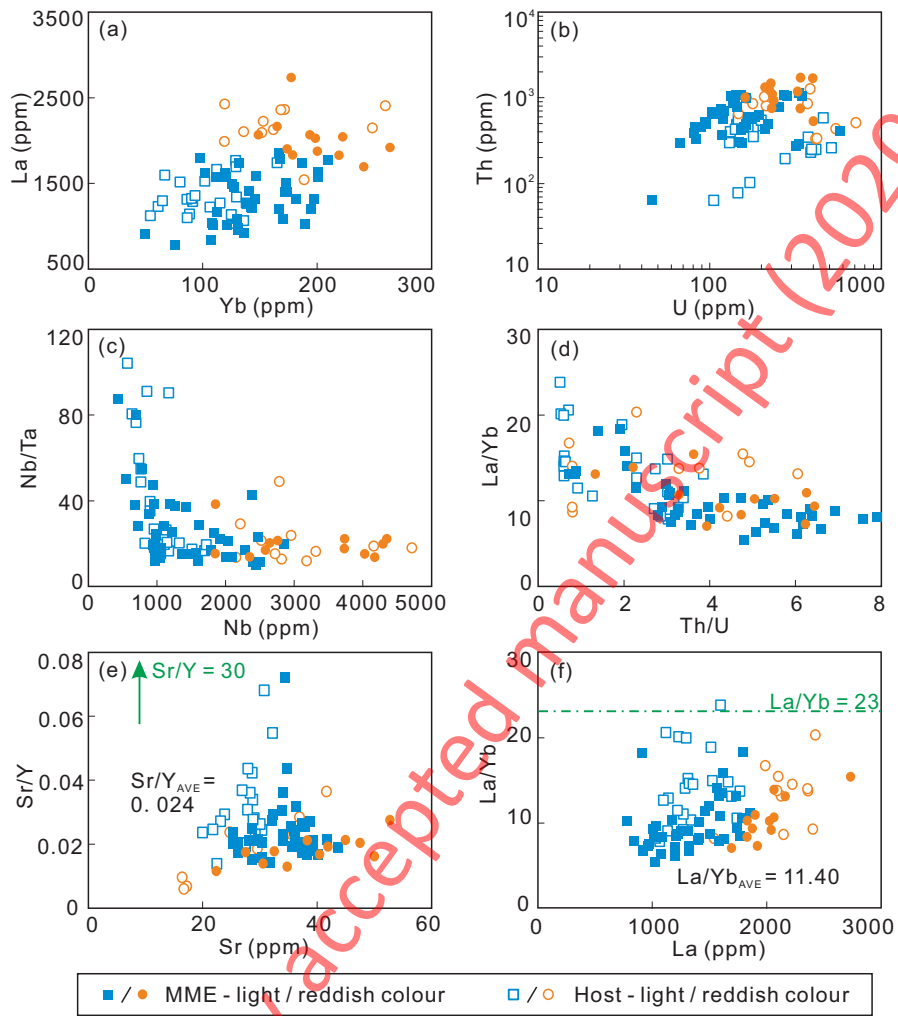


Xiao et al., Fig. 7 Titanite compositional zone



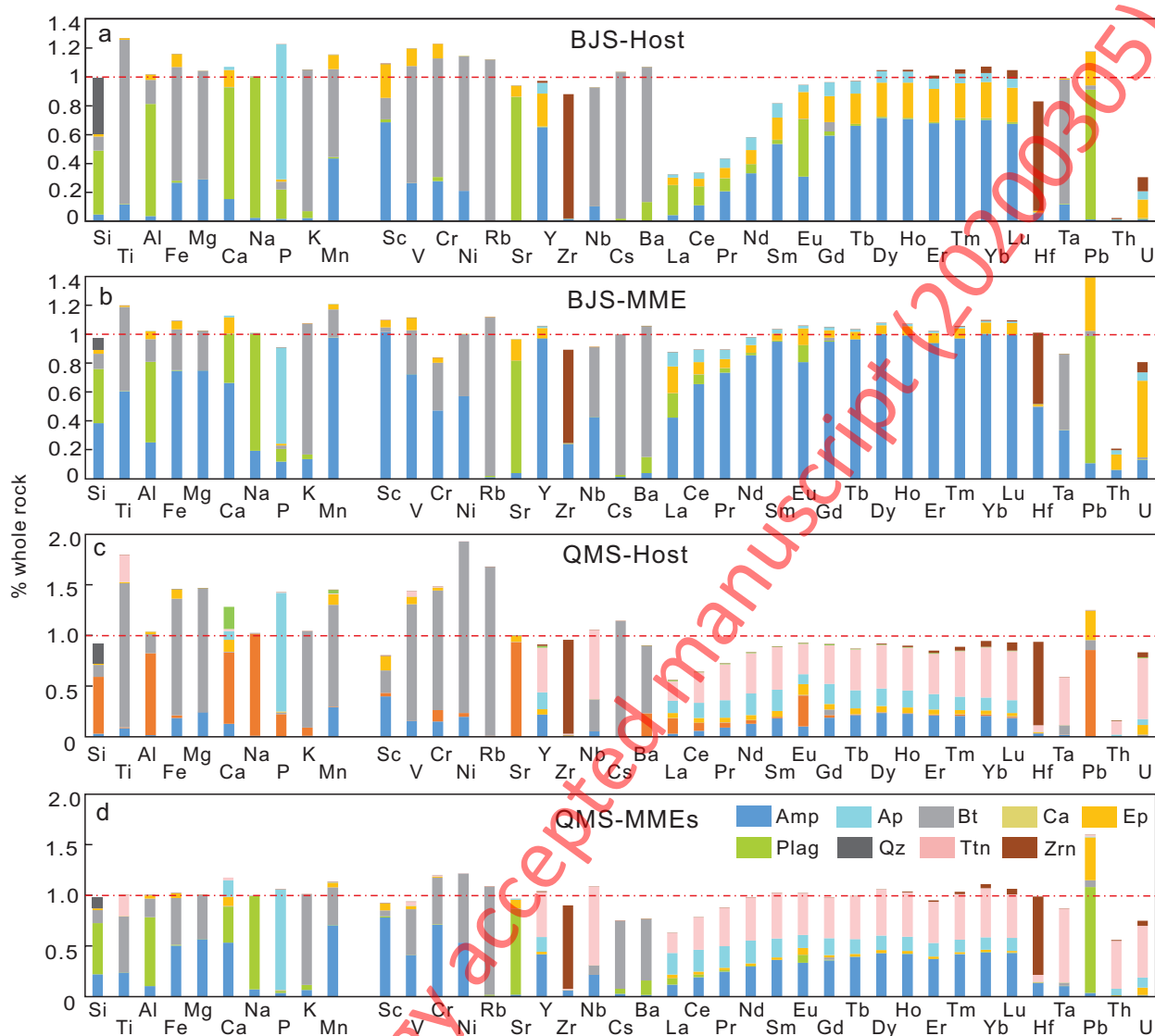
Journal of Petrology (2020) 305

Xiao et al., Fig. 8 Element co-variation for titanite

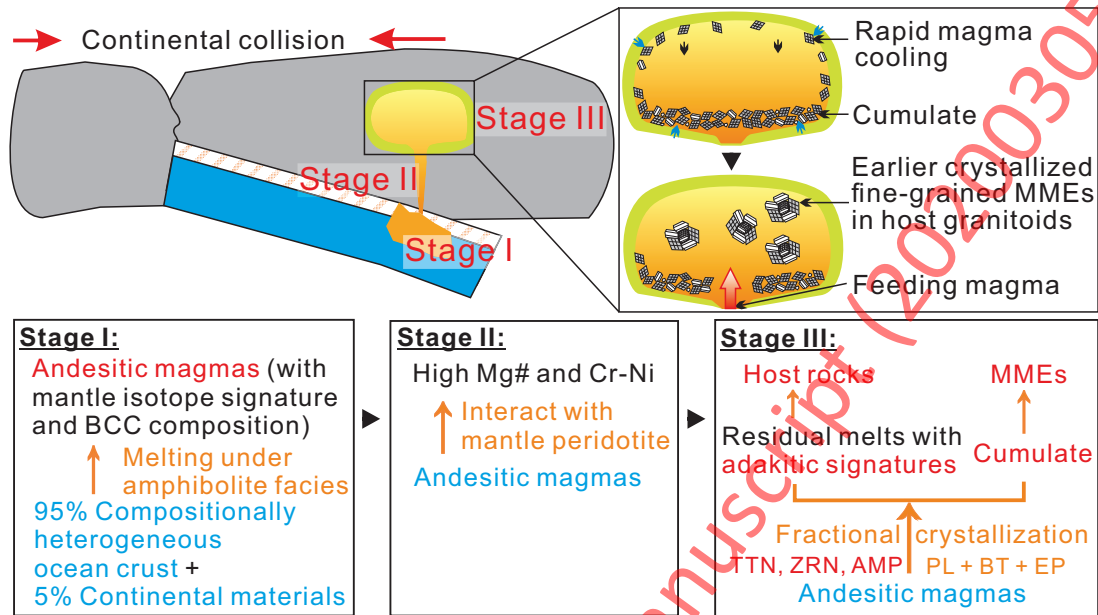


Journal of Petrology accepted manuscript (20200305)

Xiao et al., Fig. 9 Reconstructed element budgets normalized by analyzed element contents



Xiao et al., Fig. 10 Mechanism diagram for the petrogenesis of MMEs and adakitic rocks



Journal of Petrology accepted manuscript (20200305)

Xiao et al., Fig. 11 La/Yb vs. La and Sr/Y vs. Sr for minerals

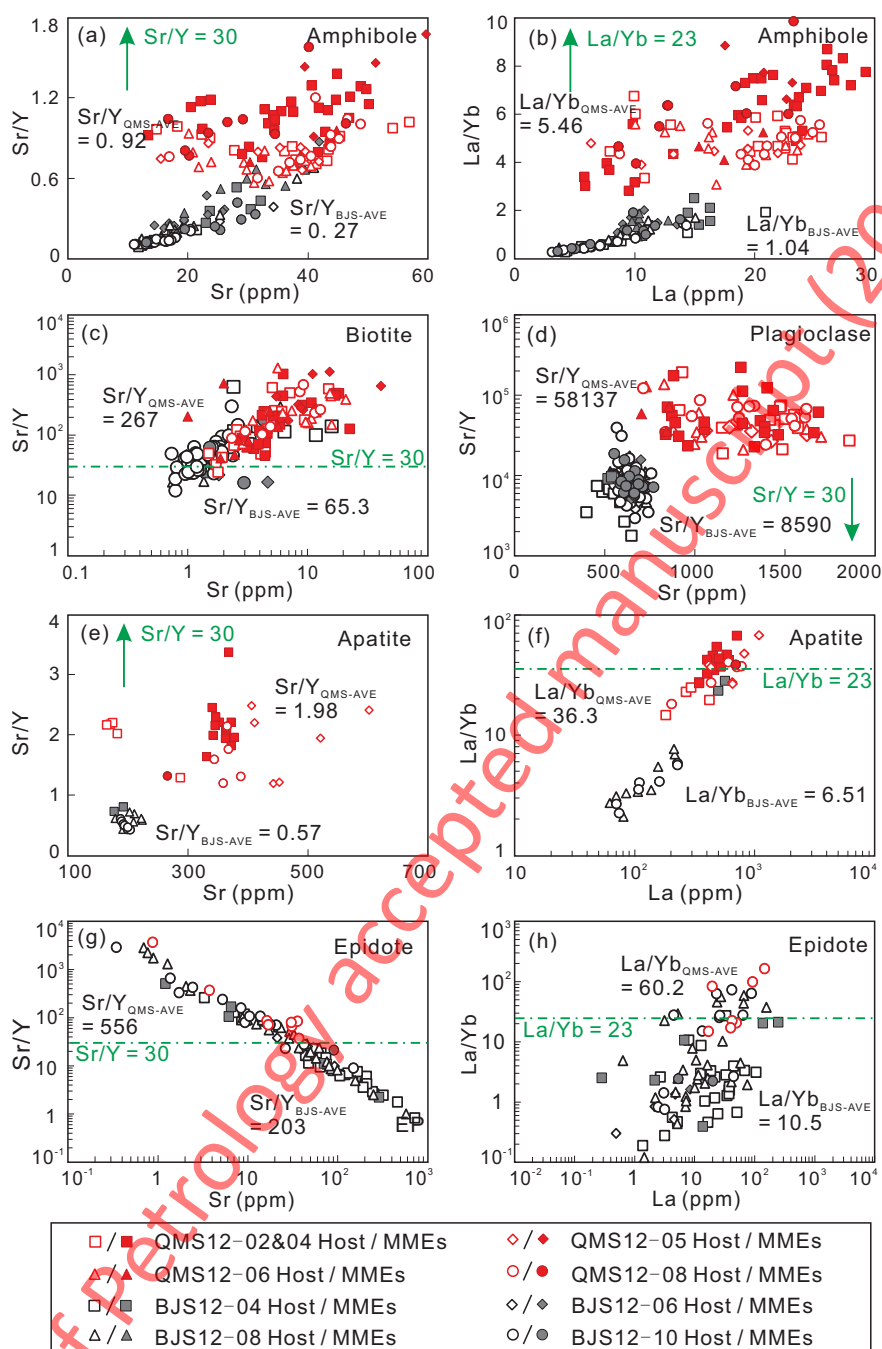


Fig. 12 Calculated melt compositions of melt in equilibrium with amphibole for two plutons

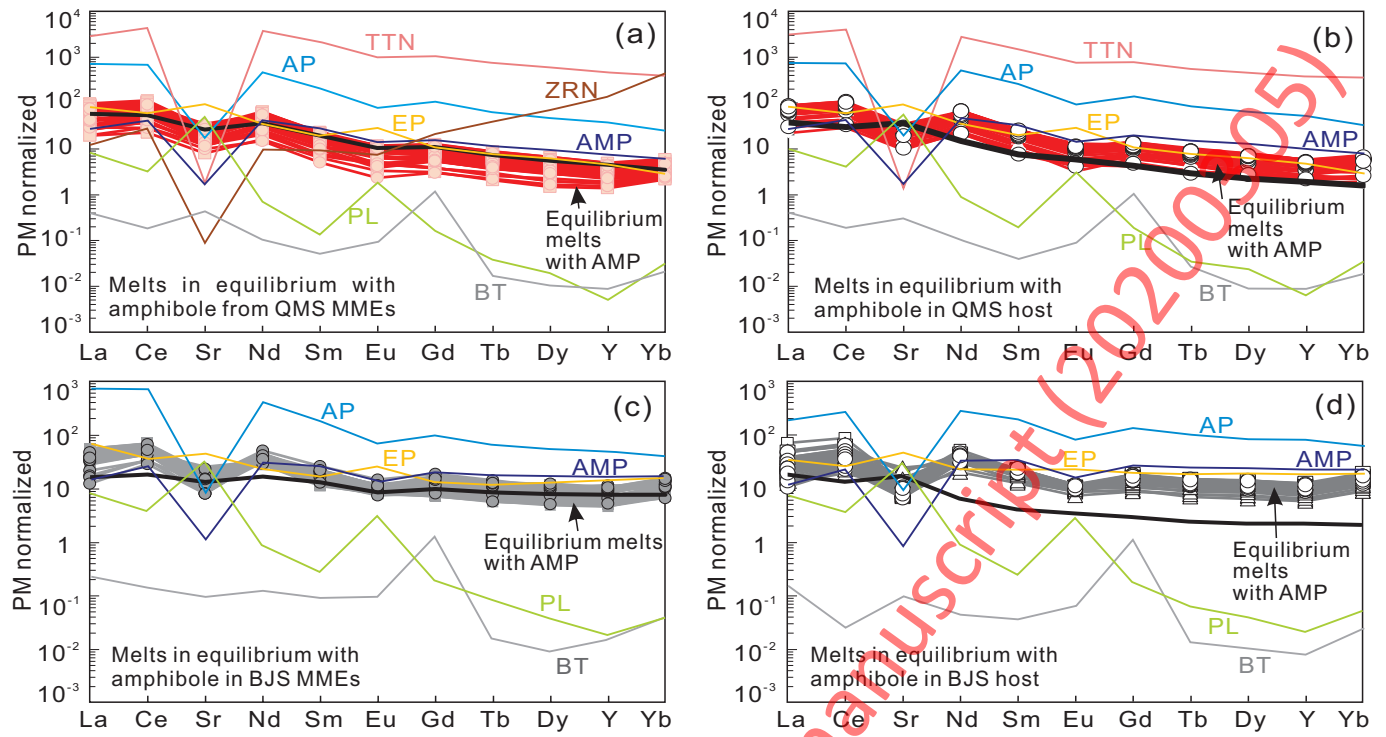
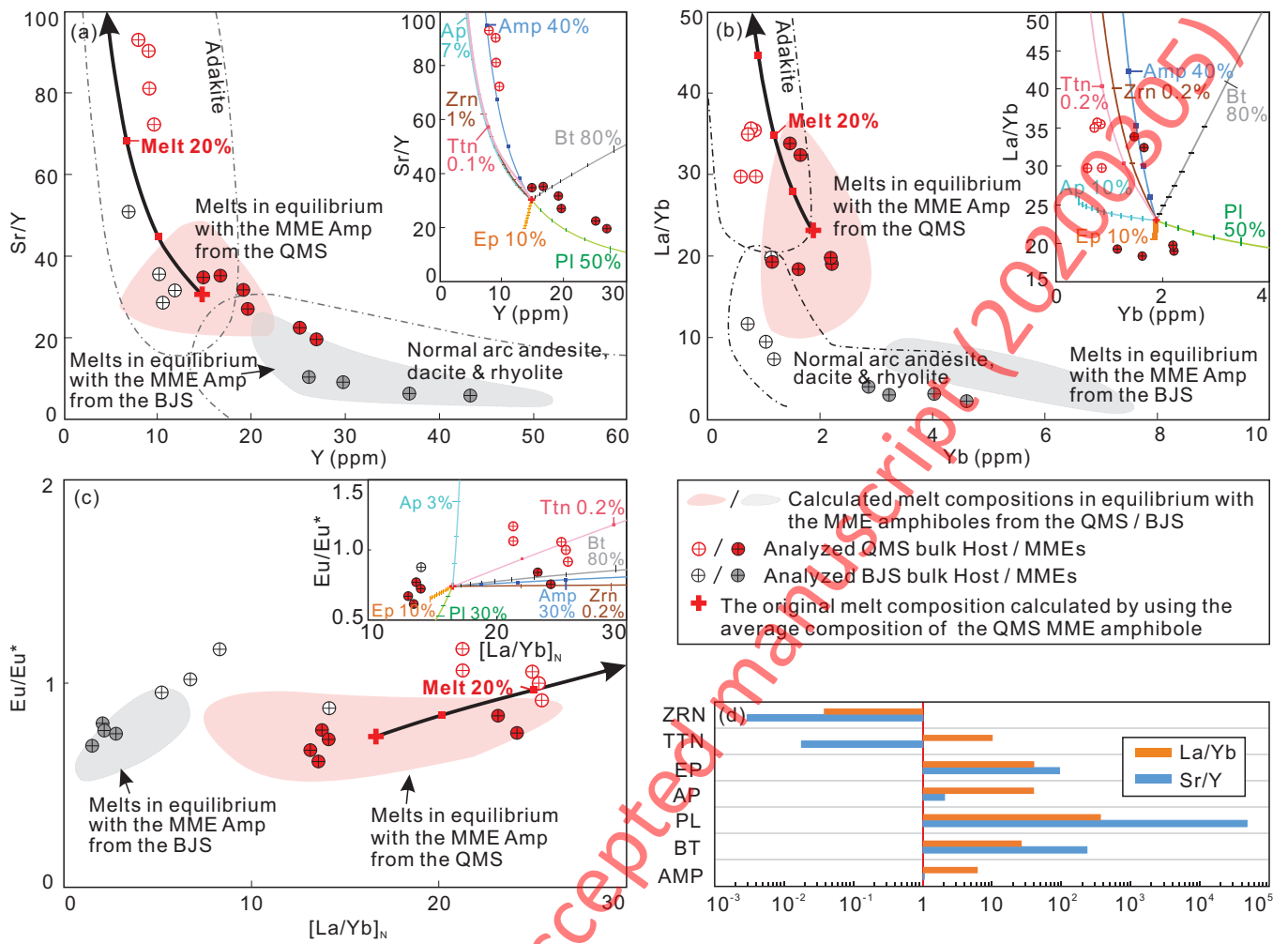


Fig. 13 Adakitic signatures of QMS host rocks



Journal of Petrology accepted manuscript 20200515